A genome-wide CRISPR-Cas9 screen identifies TGN46 as a host determinant for H-1PV susceptibility in pancreatic adenocarcinoma.

Guillaume Labrousse[1,2], Nina Suarez[1,2], Adèle Nevot[1,2], Naïma Hanoun[1,2], Nelson Dusetti[3], Louis Buscail[1,4], Claudio Murgia[2,5] and Pierre Cordelier[1,2,4,#].

1 : Univ Toulouse, CNRS, INSERM, CRCT, Toulouse, France. Equipe labellisée Fondation ARC.

2 : member of the ImCORE network.

3: Aix Marseille Univ, CNRS, INSERM, Institut Paoli-Calmettes, CRCM, Marseille, France

4: Department of Gastroenterology and Pancreatology, Toulouse-Rangueil University Hospital (CHU), Toulouse, France.

5: Building 5, Roche Pharma Research and Early Development (pRED), Roche Innovation Center, Basel, Switzerland.

*: corresponding author

Pierre Cordelier, Cancer Research Center of Toulouse (CRCT)

Team: “Therapeutic innovation in pancreatic cancer”

2, avenue Hubert Curien, 31100 Toulouse, France.

Email: pierre.cordelier@inserm.fr

Tel: +33(0)582741641

Abstract

Pancreatic ductal adenocarcinoma (PDAC) remains a highly lethal malignancy with limited response to current therapeutic strategies. Oncolytic viruses such as the rat protoparvovirus H-1PV represent promising alternatives; however, their clinical development is hindered by an incomplete understanding of virus-host interactions that determine tumor susceptibility. Here, we conducted a genome-scale CRISPR-Cas9 knockout screen in primary PDAC cultures to identify host determinants of viral infection and cytotoxicity. The screen confirmed the central role of the sialylation pathway in mediating susceptibility to H-1PV and uncovered several additional genes involved in vesicular trafficking and protein recycling. Among these candidates, *TGOLN2*, encoding the transmembrane protein TGN46, emerged as a critical host factor. Functional analyses demonstrate that TGN46 supports efficient H-1PV infection, replication, and virus-induced cytotoxicity in pancreatic cancer cells. TGN46 colocalizes with viral particles at the cell surface and facilitates their internalization through dynamin-dependent endocytosis. Molecular studies further indicate that the luminal N-terminal domain of TGN46 interacts with the viral capsid. *In vivo*, *TGOLN2* expression in essential to H-1PV-mediated antitumor activity in experimental models. Collectively, these findings identify TGN46 as a membrane-associated entry factor required for optimal H-1PV infection in PDAC cells. This work refines the mechanistic understanding of H-1PV tropism and provides a rationale for exploring host determinants of viral susceptibility as candidate biomarkers to guide parvovirus-based virotherapy.

Introduction

Pancreatic adenocarcinoma (PDAC) is notoriously resistant to therapy and difficult to cure, with a 5-year survival rate of patients less than 11%[1,2]. This poor prognosis is primarily due to the limited efficacy of current treatments, despite recent advances[3]. Most existing options, primarily chemotherapies, have shown modest benefits. In contrast, oncolytic viruses (OVs) are emerging as a promising therapeutic alternative. OVs are naturally occurring or engineered viruses that selectively infect and kill cancer cells while sparing normal tissues. They replicate within tumor cells, causing direct oncolysis and releasing tumor antigens, which can stimulate systemic anti-tumor immunity[4]. Notable example is Talimogene laherparepvec (T-VEC), an engineered herpes simplex virus approved for melanoma treatment, which has demonstrated clinical efficacy[5]. Various OVs have been investigated in preclinical and clinical settings for their ability to target and eliminate PDAC cells[6]. However, the varying efficacy of OVs in PDAC including the limited success of T-VEC[7], highlights the critical need to understand the molecular and cellular mechanisms underlying oncolytic activity. In particular, identifying host factors in tumor cells may help refine patient selection and optimize therapeutic outcomes with virotherapy.

Among the OV strains currently under investigation for PDAC, the rat H-1 protoparvovirus (H-1PV) displays particularly promising properties. H-1PV is not a human pathogen and is not associated with any known human disease. It demonstrates natural tropism and strong oncolytic activity across various cancer cell types, both *in vitro* and *in vivo* [8]. Moreover, it is well-tolerated in patients, with no severe adverse effects directly attributed to the virus, in phase I/IIa and phase II clinical trials in glioblastoma [9] and PDAC [10,11]. These findings support the potential of H-1PV as a viable candidate for oncolytic virotherapy in PDAC. H-1PV is a small, 25 nm encapsidated virus that carries a 5 kb linear single-stranded DNA genome encoding four proteins from two genes. The early P4 promoter drives expression of the non-structural (NS) proteins NS1 and NS2. NS1 is essential for viral genome replication in the host cell nucleus and activates the late P38 promoter, which controls the expression of the viral capsid proteins VP1 and VP2. These capsid proteins assemble into new virions following viral DNA packaging[12]. The oncolytic activity of H-1PV primarily relies on NS1-induced production of reactive oxygen species (ROS) and subsequent cell death resulting from DNA damage[13].

Significant efforts have been made to better understand H-1PV and its interaction with host cells. An emerging model of H-1PV entry highlights the role of the laminin γ1 chain in anchoring viral particles to the extracellular matrix (ECM)[14]. Galectin-1 (Gal-1) is also implicated in this process, cooperating with laminin during viral entry, although it does not contribute to the initial attachment of viral particles to the cell surface[14,15]. Sialic acid (SIA)

metabolism probably plays a central role in this mechanism, as H-1PV binding to laminin γ1 depends on specific SIA glycosylation motifs. Galectins can further interact with sialylated proteins to modulate viral infection, depending on the particular sialylation pattern[16]. Following attachment, H-1PV enters cells via clathrin-mediated endocytosis (CME)[17], eventually escaping from the endosomal compartment[18]. However, despite being discovered more than 60 years ago[19], a specific cellular receptor for H-1PV has yet to be identified.

In this study, we aimed to identify novel host genes involved in H-1PV infection of PDAC cells, with a particular focus on discovering candidates that may serve as potential viral receptors. We performed a genome-scale CRISPR/Cas9 knockout (KO) screen in primary PDAC cultures with intermediate sensitivity to viral infection and confirmed the essential role of the protein sialylation pathway in H-1PV susceptibility. In parallel, we identified several host genes associated with vesicular recycling, retrograde transport, and protein secretion. Among these, we focused on *TGOLN2* (Trans-Golgi Network Protein 2), which encodes TGN46, a glycosylated transmembrane protein that cycles rapidly between the cell surface and the trans-Golgi network (TGN)[20]. We demonstrated that H-1PV critically depends on TGN46 for efficient infection, replication, and cytotoxicity in primary PDAC cells. Further molecular analyses indicate that TGN46 colocalizes with H-1PV at the cell surface and facilitates rapid viral internalization in a dynamin-dependent manner. We also provide evidence that the N-terminal luminal domain of TGN46 interacts with the H-1PV capsid, in a process influenced by sialylation. Moreover, TGN46 expression associates with H-1PV permissiveness and antitumor activity in pancreatic cancer models, both *in vitro* and *in vivo*. Together, these findings identify TGN46 as a membrane-associated entry factor required for efficient H-1PV infection and refine the current understanding of parvovirus tropism. This work establishes a mechanistic basis for further exploration of host determinants as potential biomarkers of response to parvovirus-based virotherapy.

Materials and Methods

Cell culture and treatment. HeLa S3 (ATCC CCL-2™), HEK-293T (ATCC CRL-3216™), and human newborn kidney cells NB-324K (kindly provided by Dr. Jean Rommelaere, DKFZ, Heidelberg, Germany) were cultured in Dulbecco's Modified Eagle Medium (DMEM, 4.5 g/L glucose; Sigma-Aldrich, D6429) supplemented with 10% fetal calf serum (FCS; Gibco, 10270-106) and 1× antibiotic-antimycotic solution (Gibco, 15240-062). Human primary pancreatic cancer cells were maintained as previously described[21]. All cells were cultured at 37°C in a humidified atmosphere containing 5% CO_2. Doxycycline (Dox; Sigma-Aldrich, D9891) was dissolved in PBS at a stock concentration of 0.5 mM and used at a final concentration of 0.5 µM. For inducible overexpression experiments, cells were pre-treated with doxycycline at least 24 hours before seeding and continuously exposed throughout the experiment. Dynasore (Tocris Bioscience, 2897), a dynamin inhibitor, was dissolved in DMSO at a stock concentration of 25 mM and used at a final concentration of 100 µM. Cells were pre-treated for 2 hours prior to experimentation and maintained under treatment during the assay. Transferrin from human serum conjugated to Alexa Fluor™ 647 (TFn-647; Fisher Scientific, 11550766) was reconstituted in deionized water at a stock concentration of 5 mg/mL and applied to cells at a final concentration of 25 µg/mL for 5 minutes prior to fixation. For antibiotic selection, blasticidin (InvivoGen, ant-bl) was used at 0.5 µg/mL, puromycin (InvivoGen, ant-pr) at 1 µg/mL, and ouabain (Sigma-Aldrich, O3125) at 0.5 µM. Selection was carried out for a minimum of one week.

Plasmid amplification and transfection. DNA plasmid constructs used in this study were transformed and amplified in E. coli Stbl3™ competent cells (Invitrogen - C7373-03). Bacteria were plated on LB agar supplemented with the appropriate antibiotic, and individual colonies were expanded for plasmid extraction. Initial plasmid preparations were performed using the ZR Plasmid Miniprep Classic kit (Zymo Research, D4016). Clones were verified by restriction enzyme digestion and Sanger sequencing (Eurofins Genomics, LightRun). For large-scale preparations, endotoxin-free plasmid DNA was obtained using the NucleoBond Xtra Maxi kit (Macherey-Nagel, 740414.50). At each step, plasmid DNA concentration and purity were assessed using a NanoDrop spectrophotometer (ND-1000, Thermo Scientific). Cell transfections were performed using JetPRIME transfection reagent (Polyplus, 101000046) according to the manufacturer's instructions, using a DNA:JetPRIME ratio of 1:2 (µg:µL).

Virus Production. The initial stock of H-1 protoparvovirus (H-1PV) was kindly provided by Dr. Jean Rommelaere (DKFZ, Heidelberg, Germany). For virus amplification, 1.5×10^6 NB-324K cells were seeded in T175 flasks and cultured until reaching approximately 30% confluency. Cells were then infected with H-1PV at a multiplicity of infection (MOI) of 10^{-2} in 3

141 mL of infection medium (IM) consisting of Opti-MEM (Gibco, 31985-047) supplemented with
142 1% HEPES (Gibco, 15630-056) for 1 hour at 37 °C. After the adsorption period, the medium
143 was replaced with 20 mL of fresh Opti-MEM, and cells were incubated at 37 °C for 4 days
144 until the appearance of cytopathic effects (CPE). Cells were harvested by scraping into a
145 minimal volume of fresh Opti-MEM. Virions were released by three freeze–thaw cycles using
146 liquid nitrogen, followed by sonication on ice at 25 W for 30 seconds. Cellular debris were
147 removed by centrifugation at 1,800 rpm for 15 minutes, and the supernatant was filtered
148 through a 0.2 µm membrane (ClearLine, 146560). Viral stocks were aliquoted and stored at
149 −80 °C. Viral titers were determined by plaque assay on NB-324K cells as previously
150 described[22].

151 **Lentivirus production and cell transduction**. On day 1, for each lentiviral production, 4.5 ×
152 10^6 HEK-293T cells were seeded in a 100 mm dish with 10 mL of complete DMEM. On day 2,
153 HEK-293T cells were co-transfected with 6 µg of lentiviral plasmid, 4 µg of the psPAX2
154 packaging plasmid (Addgene #12260), and 1.5 µg of the pMD2.G envelope plasmid
155 (Addgene #12259) using JetPRIME reagent. Four hours post-transfection, the medium was
156 replaced with 10 mL of Opti-MEM. On day 3, target cells were seeded in 6-well plates to
157 reach 30–40% confluency by the next day. On day 4, HEK-293T supernatants were collected
158 in 50 mL tubes, centrifuged for 5 minutes at 1800 rpm to remove cell debris, and the
159 supernatant was filtered through a 0.45 µm filter (Millex-HP, SLHP033RS). Lentiviral
160 supernatants were concentrated using Vivaspin 20 columns (100 kDa MWCO PES;
161 Sartorius, VS2042) by centrifugation at 2500 rpm for 20–30 minutes. Target cells were
162 transduced with the lentiviral vectors in 2 mL of Opti-MEM supplemented with protamine
163 sulfate at a final concentration of 10 µg/mL. Forty-eight hours post-transduction, cells were
164 expanded, and appropriate antibiotic selection was initiated the following day. Selection was
165 maintained for at least one week, and cells were passaged at least twice before experimental
166 use.

167 **CRISPR knock-out screen**. The CRISPR knock-out (KO) screen methodology was adapted
168 from[23]. Briefly, PDAC087T cells were first transduced with lentiCas9-Blast (Addgene
169 #52962), enabling constitutive expression of the Cas9 enzyme and resistance to blasticidin.
170 After antibiotic selection and expansion, PDAC087T-Cas9 cells were seeded in five T175
171 flasks at 1 × 10^7 cells per flask and transduced with the GeckoV2 pooled gRNA libraries A
172 and B, inserted in the lentiGuide-Puro plasmid (Addgene #1000000049), at a multiplicity of
173 infection (MOI) of ~0.3. This low MOI maximizes the probability of integrating a single sgRNA
174 per cell while maintaining library complexity. Following one week of puromycin selection, 7.5
175 × 10^6 PDAC087T-Cas9-GeckoV2 cells were seeded in seven T175 flasks per condition (>5 ×
176 10^7 cells total). The following day, cells were incubated for 1 h at 37 °C with 5 mL infection

177 medium (IM), with or without H-1PV at MOI 10 (a dose previously shown to induce >90% cell
178 death in PDAC087T cells within 48 h). After infection, cells were washed with PBS and
179 incubated in 20 mL of complete DMEM at 37 °C. Non-infected cells were passaged at a 1:10
180 dilution upon reaching confluency. After one week, dead and floating cells were removed by
181 repeated PBS washes. Adherent cells from each condition were detached by trypsinization,
182 centrifuged, resuspended in complete medium, and pooled into one T175 flask per condition.
183 Two days later, cells were harvested again, resuspended in PBS, counted, and genomic
184 DNA was extracted using the DNeasy Blood & Tissue Kit (Qiagen #69504; one column per 5
185 × 10^6 cells, with elution in minimal volume). For each condition, sgRNA loci were amplified
186 using NGS-grade barcoded PCR primers (Eurogentec, Table 1). Amplicons were size-
187 separated by electrophoresis on 2% agarose gel, purified with the NucleoSpin Gel and PCR
188 Clean-up Kit (Macherey-Nagel #740609.250), and further cleaned using SPRIselect Beads
189 (Beckman Coulter #B24965AA). DNA fragment size was monitored at each step using a
190 Fragment Analyzer (Agilent). Once quality was confirmed, barcoded amplicons were
191 sequenced on the NextSeq 550 platform (Illumina). Sequencing data were demultiplexed
192 using the bcl2fastq algorithm (Illumina) and analyzed for sgRNA enrichment using MAGeCK
193 (Model-based Analysis of Genome-wide CRISPR-Cas9 Knockout)[24].

194 **Generation of knock-out cell lines**. To generate knock-out (KO) cell lines for individual
195 genes of interest, sgRNA protospacer sequences targeting specific loci were ordered as
196 complementary oligonucleotides. Each oligo pair was phosphorylated using T4
197 Polynucleotide Kinase (NEB #M0201) and annealed in a T100 Thermal Cycler (Bio-Rad
198 #1861096) by heating at 95 °C for 5 min, followed by a gradual temperature ramp down at
199 0.1 °C/sec to 25 °C. Subcloning of the annealed protospacer sequences was performed by
200 Golden Gate assembly. Appropriate cohesive ends were designed to enable ligation of the
201 protospacer DNA into either the lentiGuide-Puro plasmid (Addgene #52963) or the eSpCas9
202 (1.1) No FLAG ATP1 A1G2 Dual sgRNA plasmid (Addgene #86612), previously digested
203 with BsmBI (NEB #R0739) or BbsI (NEB #R3539), respectively. For validation of sgRNAs
204 identified in the CRISPR KO screen, PDAC087T-Cas9 cells were thawed and seeded in 6-
205 well plates at a density of 1.5 × 10^5 cells per well. The following day, each well was
206 transduced with a different lentiGuide-Puro construct carrying one sgRNA to validate. Cells
207 were then selected with puromycin prior to downstream use. The sequences of the sgRNAs
208 used are listed in Table 2. To generate *TGOLN2*-KO cells while avoiding constitutive
209 expression of Cas9 and sgRNA, PDAC087T and HeLa S3 cells were seeded in 6-well plates
210 at 1.5 × 10^5 cells per well and transfected the following day with 3 µg of the eSpCas9 (1.1)
211 No FLAG ATP1A1 G2 Dual sgRNA plasmid. This construct expresses Cas9 along with a
212 sgRNA targeting exon 3 of *TGOLN2*. To enrich for successfully edited cells, the plasmid also

213 contains a second sgRNA targeting exon 4 of the ATP1A1 gene, an essential gene whose
214 disruption confers resistance to ouabain, a cytotoxic drug. This strategy selectively enriches
215 cells that have undergone mutagenic repair at the ATP1A1 locus without impairing its
216 function[25]. For generation of TGN46-WT control cells undergoing the same transfection and
217 selection process, a similar construct expressing only the ATP1A1-targeting sgRNA was
218 transfected in parallel. Five days post-transfection, ouabain was added to the culture
219 medium. After one week of recovery, *TGOLN2* KO efficiency was assessed by Western blot
220 and immunofluorescence.

221 ***TGOLN2* cDNA cloning**. Total mRNA from PDAC087T cells was extracted using the
222 RNeasy Plus Mini Kit (Qiagen #74134) and reverse-transcribed into complementary DNA
223 (cDNA) with the RevertAid Kit (Thermo Fisher #K1691). The resulting cDNA was used as a
224 template for high-fidelity PCR amplification of the open reading frame (ORF) corresponding
225 to the main *TGOLN2*-201 spliced variant (Ensembl transcript ID: ENST00000377386.8),
226 which encodes the 437-amino acid TGN46 protein (6050 bp). PCR amplification was
227 performed using PrimeSTAR Max DNA Polymerase (Takara #R045A). To facilitate
228 downstream cloning, gene-specific primers containing restriction sites were used: an AvrII
229 site at the 5' end and a MluI site at the 3' end. The sequences were as follows: Forward: 5′-
230 TTTACGCGTttaggacttctggtccaaac-3′, Reverse: 5′-TTTCCTAGGgccaccatgcggttcgtggttgcctt-
231 3. The PCR product was purified using the NucleoSpin Gel and PCR Clean-up Kit
232 (Macherey-Nagel), digested for 1 h at 37 °C with AvrII and MluI restriction enzymes (NEB
233 #R3198, #R0174), and re-purified before ligation into a similarly digested third-generation
234 lentiviral vector, pLIX402 (Addgene #41394), to generate the pTRE- *TGOLN2* construct. This
235 all-in-one plasmid contains the complete Tet-On system, including a constitutive expression
236 cassette encoding the rtTA-3 transactivator, followed by a 2A self-cleaving peptide and the
237 puromycin resistance gene. Upon doxycycline (dox) treatment, rtTA-3 binds to the TRE
238 (tetracycline-responsive element) promoter, thereby inducing the expression of TGN46.

239 ***TGOLN2* mutagenesis and fusion with EGFP and FLAG tags.** TGN46 deletion constructs,
240 TGN46-ΔI, TGN46-ΔII, and TGN46-ΔIII, were generated by high-fidelity PCR using the
241 pTRE- *TGOLN2* plasmid as a template. Each deletion targeted specific domains of the
242 protein as described in Illustration 1, and the oligonucleotides used for amplification are listed
243 in Table 3. To facilitate detection and localization studies, EGFP or FLAG (DYKDDDDK) tags
244 were fused either to the N- or C-terminus of TGN46. Importantly, N-terminal tags were
245 inserted immediately downstream of the signal peptide sequence to preserve the protein's
246 tethering to the secretory pathway. The tagged and truncated TGN46 variants were
247 subcloned into the pLIX402 lentiviral vector (Addgene #41394) using standard molecular
248 cloning techniques detailed in Illustration 1. Lentiviral particles were produced using these

249 constructs, and PDAC087T- *TGOLN2*-KO cells were transduced accordingly. After
250 puromycin selection, cells expressing the tagged or truncated TGN46 variants were used in
251 rescue experiments.

252 **Protein extraction and Western Blot analysis**. For protein extraction, cultured cells grown
253 in 100 mm dishes were washed with ice-cold PBS after removal of the culture medium. PBS
254 was then aspirated, and cells were lysed directly on ice for 10 minutes with 200 µL of RIPA
255 Buffer II, pH 8.0 (Bio Basic – RB4476) supplemented with protease inhibitor cocktail (Sigma-
256 Aldrich – P8340). Lysates were scraped on ice and collected in 1.5 mL microcentrifuge tubes.
257 Cell lysates were sonicated (e.g., 3 cycles of 5 seconds ON / 10 seconds OFF at 30%
258 amplitude using a probe sonicator; adjust based on equipment), followed by centrifugation at
259 13,000 × g for 10 minutes at 4 °C. The clarified supernatants were transferred to fresh tubes,
260 and protein concentrations were determined using the Bradford reagent (SERVA –
261 39222.03). A fixed amount of protein (30 to 80 µg per sample) was denatured in Laemmli
262 buffer by heating at 95 °C for 5 minutes, then immediately loaded on 10–12% SDS-
263 polyacrylamide gels (Sigma-Aldrich – A3699). Electrophoresis was performed using TG-SDS
264 running buffer (Euromedex – EU0510). Proteins were transferred to nitrocellulose
265 membranes using the Trans-Blot® Turbo™ RTA Transfer Kit and Transfer System (Bio-Rad
266 – 1704271 and 1704150EDU). Transfer efficiency was verified by Ponceau S staining.
267 Membranes were blocked for 30 minutes at room temperature (RT) on a rocking platform in
268 TBS-T (TBS with 0.1% Tween-20; Sigma-Aldrich – P1379) containing 5% non-fat dry milk
269 (Millipore – 70166). After blocking, membranes were incubated overnight at 4 °C with primary
270 antibodies diluted in TBS-T + 1% milk, according to the manufacturers' recommendations.
271 The next day, membranes were washed three times for 10 minutes at RT in TBS-T, then
272 incubated for 1 hour at RT with secondary HRP-conjugated antibodies diluted in TBS-T + 1%
273 milk. After washing again (3×10 min, RT), detection was performed using the Clarity Western
274 ECL substrate (Bio-Rad – 170-5061), and signal acquisition was carried out with the
275 ChemiDoc™ XRS+ System and Image Lab™ Software (Bio-Rad – 1708265). All antibodies
276 used, along with their sources and working dilutions, are listed in Table 4. Rabbit antisera
277 against H-1PV NS1 and VP were generously provided by Dr. Jürg Nüesch (DKFZ,
278 Heidelberg, Germany)[26].

279 **Viability assays**. Cells were seeded in white-bottom 96-well plates (Greiner Bio-One –
280 675075) at a density of 1×10^4 cells per well in 100 µL of complete medium, in the presence
281 or absence of dox. The following day, cells were incubated for 1 hour at 37 °C with 25 µL of
282 infection medium containing or not H-1PV, applied across 10 different MOIs using a 1:2
283 serial dilution series starting from MOI 100 down to MOI 0.19. Following incubation, wells
284 were washed once with PBS, and 100 µL of fresh complete medium (± dox) was added. At

285 48 hours post-infection, 100 µL of CellTiter-Glo® Luminescent Cell Viability reagent
286 (Promega – G7572) was added per well. Plates were mixed for 2 minutes on an orbital
287 shaker to ensure complete cell lysis and reagent mixing. Luminescence was measured as
288 Relative Luminescence Units (RLU) using a TriStar² LB 942 plate reader (Berthold
289 Technologies). For normalization, non-infected control wells were used to define 100%
290 viability, and values from infected conditions were expressed as percentages relative to this
291 reference.

292 **Cell counting**. Cells were seeded in 24-well plates at a density of 4.5×10^4 cells per well in
293 0.5 mL of complete DMEM, with or without dox. For each condition, four replicate wells were
294 prepared, and a separate plate was used for each time point (4 h, 24 h, 48 h, and 72 h). The
295 following day, cells were incubated for 1 hour at 37 °C with 250 µL of infection medium (IM),
296 in the presence or absence of H-1PV, at MOIs of 2.5 or 10. After incubation, wells were
297 washed three times with PBS, and 0.5 mL of fresh complete medium (± dox) was added. For
298 cell counting, 200 µL of the cell suspension was diluted in 20 mL of ISOTON II diluent
299 (Beckman Coulter – 8448011) and analyzed using a Coulter Z1 Particle Counter (Beckman
300 Coulter).

301 **Viral genome quantification by RT(q)PCR**. To assess virus production by infected cells,
302 cells were seeded in 24-well plates at a density of 4.5×10^4 cells per well in 0.5 mL of
303 complete DMEM, with or without doxycycline (dox). For each condition, four replicate wells
304 were prepared, and a separate plate was used for each time point (4 h, 24 h, 48 h, and 72 h).
305 The following day, cells were incubated for 1 hour at 37°C with 250 µL of infection medium,
306 in the presence or absence of H-1PV, at MOIs of 2.5 or 10. After incubation, wells were
307 washed three times with PBS, and 0.5 mL of fresh complete medium (± dox) was added. At
308 each indicated time point, supernatants were collected and diluted 1:2 in PBS in individual
309 1.5 mL tubes for analysis of released virus. To monitor intracellular viral genome
310 accumulation, cells were seeded in 24-well plates at a density of 2×10^5 cells per well in 0.5
311 mL complete DMEM ± dox, aiming for a full monolayer by the next day. Plates were prepared
312 with four replicate wells per condition, and a dedicated plate was used for each time point (15
313 min, 1 h, 2 h, and 4 h). Cells were infected with 250 µL of IM ± dox, ± H-1PV at MOIs of 2.5
314 or 10. At each time point, supernatants were aspirated, cells were washed four times with
315 PBS, and detached with 250 µL trypsin for 5 minutes at 37°C. The reaction was stopped by
316 adding 250 µL of complete DMEM, and cells were thoroughly dissociated. Four hundred
317 microliters of each cell suspension were diluted in 600 µL PBS (cell fraction) and transferred
318 into 1.5 mL microtubes. Samples (1 mL total) were freeze-thawed three times using liquid
319 nitrogen, then centrifuged at 12,000 × g for 10 minutes at 4°C. Supernatants were collected
320 for qPCR analysis. For quantification of viral genomes, MicroAmp™ Fast Optical 96-Well

321 Reaction Plates (Invitrogen – 4346906) were filled with 18 µL of qPCR mix, composed of 10
322 µL SsoFast™ EvaGreen® Supermix (Bio-Rad – 1725204), 0.66 µL of each oligonucleotide
323 (10 µM): Forward: 5′-GCGCGGCAGAATTCAAACT-3′ and Reverse: 5′-
324 CCACCTGGTTGAGCCATCA-3′, and 7.88 µL DNAse/RNAse-free water. Then, 2 µL of each
325 sample was added to individual wells. A standard curve was generated using serial dilutions
326 of the pSR19 plasmid, kindly provided by Dr. Jean Rommelaere, which contains the full H-
327 1PV genome. Known copy numbers of pSR19 were used to calculate genome copy numbers
328 in each sample. Fast RT-qPCR was performed using the StepOnePlus™ Real-Time PCR
329 System (Applied Biosystems – 4376600), and data were analyzed with StepOne Software
330 v2.3.

331 **Immunofluorescence and viral proteins detection**. Cells were seeded in 24-well plates at
332 a density of 4.5×10^4 to 8×10^5 cells per well on 14mm coverslips (Knittel Glass - 100041)
333 with 1 mL of complete DMEM, with or without dox, and incubated at 37°C. The following day,
334 cells were incubated for 1 hour at 37°C with 250 µL of infection medium, in the presence or
335 absence of H-1PV at MOIs of 1 or 2.5. After the incubation, the cells were washed three
336 times with PBS and replaced with 1 mL of complete medium (± dox) and incubated for an
337 additional 24 hours at 37°C. At the end of the incubation, cells were washed with PBS and
338 fixed with PBS-PFA 4% (Electron Microscopy Science - 15710) for 15 minutes at room
339 temperature. After fixation, cells were washed three times with PBS, permeabilized with
340 PBS-Triton X-100 0.25% (Sigma-Aldrich - 93443) for 20 minutes at room temperature,
341 washed three times with PBS, and blocked in PBS-BSA 5% (Euromedex - 04-100-812-E) for
342 30 minutes at room temperature. For the immunodetection of proteins of interest, cells were
343 incubated with primary antibody diluted in 200 µL of PBS-BSA 1% for 2 hours at room
344 temperature with stirring. After primary antibody incubation, cells were washed three times
345 for 5 minutes with PBS and then incubated with secondary antibody diluted in 200 µL of
346 PBS-BSA 1% for 1 hour at room temperature with stirring. Cells were then incubated with
347 PBS containing DAPI at 0.5 µg/mL (Euromedex - 1050A) for 10 minutes at room
348 temperature. After DAPI staining, cells were washed three times for 5 minutes with PBS.
349 Finally, cells were mounted on glass slides with 10 µL of fluorescent mounting medium (Dako
350 - 53023). Image acquisition was performed using a widefield microscope (ZEISS -
351 AxioObserver Z1) with a 10X objective or a confocal microscope (ZEISS - LSM880 Fast
352 Airyscan) with a 63X objective. Images were analyzed with ImageJ 1.53o software. DAPI
353 staining was used to determine the number of cells per field, and fluorescence intensity and
354 area were normalized accordingly. All antibodies used, including dilutions, are listed in
355 Tablexxx. Rabbit antisera directed against H-1PV capsid were kindly provided by Dr. Jürg
356 Nüesch (DKFZ, Heidelberg, Germany).

357 **Viral particles co-localization studies and binding kinetics**. For co-localization studies,
358 cells were seeded in 24-well plates at a density of 4.5×10^4 cells per well on 14 mm
359 coverslips, in 1 mL of complete DMEM supplemented with or without dox, and incubated for
360 48 hours at 37 °C. To assess viral entry, cells were pre-incubated for 15 minutes on ice,
361 followed by a 1-hour incubation on ice with 250 µL of infection medium containing H-1PV at a
362 MOI of 250, in the presence or absence of dox. Cells were transferred to 37 °C to allow
363 synchronized viral entry. For binding kinetic assays, cells were first incubated for 2 hours at
364 37 °C with 0.5 mL of complete DMEM, with or without dox, and with or without hydroxy-
365 dynasore, a dynamin inhibitor. Cells were then incubated with 250 µL of IM supplemented
366 with the same conditions (± dox, ± hydroxy-dynasore) and H-1PV at a MOI of 250, and
367 maintained at 37 °C. At various time points ranging from 0 minutes to 4 hours post-infection,
368 cells were extensively washed with PBS to remove unbound virus and immediately
369 processed for immunofluorescence staining, as described previously.

370 **GFP-Trap**. On day 0, cells were seeded in 100 mm dishes at a density of 1.5×10^6 cells per
371 dish in 10 mL of complete DMEM supplemented with doxycycline. On day 1, H-1PV was
372 added directly to the culture medium at a MOI of 2.5. On day 4, protein extraction was
373 performed as previously described. GFP-Trap was then carried out using agarose beads
374 coupled with highly specific anti-GFP nanobodies (Proteintech – gta), following the
375 manufacturer's instructions. Briefly, cell lysates were diluted with 300 µL of dilution buffer
376 (10 mM Tris-HCl, 150 mM NaCl, 0.5 mM EDTA, pH 7.5) supplemented with 25 µL of GFP-
377 Trap beads, and incubated for 1 hour at 4 °C on a rotating wheel. Beads were collected by
378 centrifugation at 2,500 × g for 2 minutes at 4 °C and washed four times with wash buffer
379 (dilution buffer supplemented with 0.05% NP-40) to remove unbound proteins. Finally, bead-
380 bound proteins were eluted by heating for 5 minutes at 95 °C in 2X Laemmli buffer. For
381 Western blot analysis, 50 µL of input lysate (I), flow-through (FT, unbound proteins), and
382 bead-bound fraction (B) were loaded per sample.

383 **Statistics and Reproducibility.** No sample size calculation was performed. All experiments
384 were conducted with at least three biologically independent replicates, and each experiment
385 included a minimum of three technical replicates. No data were excluded from the analysis.
386 Calculations were performed using Microsoft Excel Professional Plus 2016. Statistical
387 analyses were carried out using GraphPad Prism version 10.1.2. For comparisons involving
388 two or fewer groups, unpaired two-tailed Student's t-tests were used. For comparisons
389 involving more than two groups, ordinary one-way ANOVA was performed. In both cases, a
390 95% confidence interval was applied. In micrographs, p-values are indicated as follows: ns
391 for non-significant ($p > 0.05$), * for $p \leq 0.05$, ** for $p \leq 0.01$, *** for $p \leq 0.001$, and **** for $p \leq$

392 0.0001. Unless otherwise specified, error bars on micrographs represent standard deviation
393 (S.D.).

394 **Data availability**. All data generated or analyzed during this study are included in this
395 published article and its supplementary information files. Access to raw data will be made
396 available upon reasonable request to the corresponding author.

397 **Competing interests**. CM is employee of F. Hoffmann-La Roche. The other authors declare
398 no competing interests.

399

Results

CRISPR/Cas9 KO screen identifies host genes for H-1PV infection in PDAC cells. To uncover host factors essential for H-1PV infection, we performed a genome-wide CRISPR-Cas9 knockout screen using the lentiviral GeckoV2 sgRNA library in the PDAC087T primary pancreatic cancer primary culture (Fig. 1A). This model was selected for its biological relevance, robust proliferation, amenability to lentiviral transduction, and susceptibility to H-1PV-mediated oncolysis. Following Cas9 expression and library transduction, cells were either mock-treated or infected with H-1PV. Genomic DNA was extracted one week post-infection, and integrated sgRNA sequences were PCR-amplified and subjected to next-generation sequencing. MAGeCK analysis identified 19 candidate genes whose loss conferred resistance to H-1PV infection (Fig. 1B). To validate these candidates, we conducted a secondary screen in which each gene was targeted using two independent sgRNAs expressed transiently. Three non-targeting sgRNAs served as negative controls. Transfected cells were challenged with H-1PV, and cell viability was quantified 48 hours later (Fig. 1C-D). Knockout of *GAD2*, *MSLN*, *CORO7*, and *ACTL7B* did not significantly alter sensitivity to H-1PV, suggesting these represent false positives or context-dependent hits. In contrast, loss of *SLC35A1*, *SLC35A2*, *CMAS*, *ST3GAL4*, *TGOLN2*, *UNC50*, *GOSR1*, *VPS51*, *VPS54*, *PTAR1*, *COG1*, *COG3*, *COG4*, or *SEC61B* led to reproducible protection from virus-induced cytotoxicity in at least one sgRNA per gene, supporting their functional involvement in H-1PV infection.

To gain insight into the functional landscape of candidate H-1PV host factors, we conducted gene ontology enrichment analysis using the PANTHER classification system (Table 5). This analysis highlighted several significantly enriched biological processes, including nucleotide sugar transport, retrograde trafficking at the trans-Golgi network (TGN), intra-Golgi vesicular transport, sialic acid metabolism, and coatomer protein complex I (COPI)-mediated anterograde transport from the endoplasmic reticulum (ER) to the Golgi apparatus. Notably, many identified genes are involved in vesicle-mediated trafficking, suggesting a model in which H-1PV co-opts host transport machinery for efficient intracellular trafficking and infection. Among the candidate genes, we focused on *TGOLN2*, which encodes the glycoprotein TGN46, a conserved sialylated glycoprotein predominantly localized to the TGN, where it functions in the sorting of cargo destined for secretion[20]. Furthermore, a fraction of TGN46 also traffics to the plasma membrane, where it interfaces with components of clathrin-mediated endocytosis (CME)[27], a process that was shown to be critical for efficient H-1PV entry[17]. Given the strong protective phenotype observed upon *TGOLN2* knockout (Fig. 1C-D) and its known roles in endocytic and secretory pathways, we hypothesized that

435 TGN46 facilitates a key step in H-1PV entry or intracellular trafficking, warranting further
436 mechanistic investigation.

437 ***TGOLN2* knockout and overexpression models demonstrate a strong dependency of**
438 **H-1PV on TGN46 for successful infection.**

439 To determine whether TGN46 is required for H-1PV infection, we first performed loss-of-
440 function experiments using gene knockout (KO). We generated PDAC087T cells deficient for
441 *TGOLN2* (PDAC087T-KO) using a non-integrative strategy to minimize permanent genetic
442 alterations and reduce off-target effects associated with constitutive Cas9 expression[28] (Fig.
443 S1A). Efficient TGN46 depletion was confirmed at the protein level by western blotting (Fig.
444 S1B) and immunofluorescence (Fig. S1C). PDAC087T-KO cells demonstrated complete
445 protection from infection at MOI 2.5 or 10 (Fig. 2A), whereas control cell numbers decreased
446 by 35% ± 9% ($p < 0.004$) and 67% ± 9% ($p < 0.001$), respectively (Fig. 2A). We next
447 extended this analysis to HeLa cervical cancer cells, a model known to be permissive to H-
448 1PV infection[29]. Western blot confirmed the *TGOLN2* KO (Fig. S1D). Viability assays
449 performed 48 hours post-infection showed that *TGOLN2* KO resulted in a significant
450 reduction in H-1PV-induced oncolysis compared with their respective control cells (Fig. S1E),
451 indicating that TGN46 may function as a conserved host factor for H-1PV infection. We then
452 measured viral genome content in wt and PDAC087T-KO cells following infection with H-
453 1PV. Consistent with the reduction in oncolysis, viral replication was strongly impaired in the
454 absence of TGN46. Quantification of viral DNA by qPCR revealed a significant decrease in
455 intracellular H-1PV genome copies in *TGOLN2*-deficient cells compared with controls (-94%
456 ± 0.5%, $p < 0.01$ and -82% ± 5.6%, $p < 0.001$ for MOI 2.5 and MOI 10, respectively; Fig. 2B).
457 To assess whether this defect translated into altered production of infectious viral particles,
458 we next quantified extracellular H-1PV virions in culture supernatants. TGN46-deficient
459 PDAC087T cells released significantly fewer viral particles compared with control cells, as
460 measured by qPCR-based particle quantification (-73% ± 31%, $p < 0.001$, and -71% ± 11%,
461 $p < 0.001$, at MOI 2.5 and MOI 10, respectively Fig. 2C). These findings indicate that TGN46
462 loss impairs intracellular viral genome amplification and limits productive virion generation.
463 We next assessed viral protein expression by immunofluorescence. In control cells, robust
464 expression of NS1 and capsid viral protein was readily detected, with a characteristic
465 intracellular distribution (Fig. 2D-E). In contrast, *TGOLN2*-deficient cells consistently
466 displayed a marked reduction in the proportion of infected cells (-74% ± 18%, $p < 0.001$ for
467 NS1 and -85% ± 11%, $p < 0.001$ for capsid proteins, respectively Fig. S1F-G), consistent
468 with impaired viral gene expression. We then assessed whether TGN46 overexpression was
469 sufficient to modulate viral infection and efficacy. To this end, we established PDAC087T
470 cells in which TGN46 overexpression is induced upon doxycycline (dox) treatment (Fig.

471 S1H). Western blotting (Fig. S1I) and immunofluorescence (Fig. S1J) for TGN46 validated
472 both cellular models. We next assessed the impact of TGN46 overexpression following
473 infection with H-1PV at various MOI. Proliferation assays indicated that doxycycline
474 treatment did not affect cell growth, and revealed that TGN46 overexpression resulted in
475 25% ± 4% ($p < 0.004$) and 31% ± 4% ($p < 0.03$) reduced viability at MOI 2.5 and 10,
476 respectively (Fig. 2F). Furthermore, intracellular viral genome content was significantly higher
477 in cells overexpressing TGN46, compared with control cells, with a 2.4 ± 0.2-fold ($p < 0.01$)
478 and 1.5 ± 0.3-fold ($p < 0.002$) increase at MOI 2.5 and 10, respectively (Fig. 2G). In contrast,
479 viral genome levels detected in the culture supernatant, reflecting released progeny virions,
480 were not significantly altered (Fig. 2H). Together, these findings are consistent with a role for
481 TGN46 in early stages of the H-1PV infectious cycle rather than in late steps of virion
482 production or release. Finally, Immunofluorescence analysis further showed enhanced viral
483 protein expression upon TGN46 overexpression. Twenty-four hours post-infection at MOI
484 2.5, TGN46-overexpressing cells exhibited a significant increase in the percentage of NS1
485 (1.7-fold ± 0.5, $p<0.05$, Fig. 2I and Fig. S1K) and conformed viral capsid-positive cells (3.6-
486 fold ± 0.9, $p<0.01$, Fig. 2J and Fig. S1L) compared with controls, consistent with increased
487 viral gene expression and productive infection. Taken together, these complementary loss-
488 and gain-of-function experiments identify *TGOLN2*/TGN46 as a host factor that promotes
489 productive H-1PV infection, consistent with a role at an early stage of the viral life cycle,
490 potentially at or upstream of viral entry.

491 **TGN46 regulates H-1PV entry and co-localizes with H-1PV virions at the cell**
492 **membrane.** Given TGN46's involvement in protein secretion and vesicular recycling, we
493 sought to determine whether its role in H-1PV infection might be indirect, affecting
494 endocytosis pathways, or if TGN46 directly contributes to the virus's attachment or entry into
495 cells. To investigate this, we performed immunofluorescence analyses to assess the steady-
496 state levels of major endocytosis markers of CME in both PDAC087T-KO and PDAC087T
497 cells overexpressing TGN46. Confocal microscopy images were analysed to quantify
498 expression levels, vesicle numbers, and average vesicle sizes using Clathrin Heavy Chain
499 (CHC), Rab5a (early endosome marker), EEA1 (early-intermediate endosome marker), and
500 LAMP1 (lysosomal marker). Single-cell quantification revealed that *TGOLN2* knockout or
501 overexpression did not generally alter the expression levels of these endocytic markers, with
502 the exception of EEA1, whose relative signal was increased in *TGOLN2*-depleted cells (Fig.
503 S2A-B). *TGOLN2* downregulation also induced significant changes in both the number (CHC,
504 Rab5a, EEA1) and size (CHC, Rab5a, EEA1) of endocytic vesicles, whereas TGN46
505 overexpression had no detectable effect. To assess whether these morphological alterations
506 affected CME functionality, we performed transferrin uptake assays using Alexa-647-

507 conjugated transferrin (TFn-647), which is internalized exclusively via CME[30]. After a 5-
508 minute incubation, no differences in total TFn-647 uptake were observed between *TGOLN2*
509 knockout, TGN46-overexpressing, and wild-type cells (Fig. S2A-B). However, the number of
510 transferrin-positive vesicles was reduced in *TGOLN2*-depleted cells. Together, these data
511 indicate that modulation of TGN46 expression does not impair the overall capacity for CME
512 in PDAC087T cells.

513 Based on these observations, we next investigated whether TGN46 plays a specific role
514 during the early stages of H-1PV entry. To address this, we performed an H-1PV
515 internalization assay. PDAC087T cells were incubated with H-1PV, and at the indicated time
516 points, cells were washed to remove unbound virus (Fig. 3A). Viral genome content was then
517 quantified by qPCR. At 2 hours post-infection, *TGOLN2*-KO cells contained 45% fewer viral
518 genomes than wild-type controls (Fig. 3A, $p<0.005$), whereas TGN46-overexpressing cells
519 exhibited more than a twofold increase in viral genome levels as early as 15 minutes post-
520 infection (Fig. 3B). These results indicate that TGN46 enhances early H-1PV entry in a dose-
521 dependent manner. To further investigate the role of TGN46 during H-1PV entry, we adapted
522 a previously described synchronization protocol[17] to visualize the interaction between TGN46
523 and H-1PV using an antibody recognizing conformational capsid epitopes in intact virions.
524 Vesicular trafficking was transiently inhibited in PDAC087T cells by incubation at 4°C for 15
525 minutes, followed by exposure to a high viral input (MOI 250) for 1 hour at 4°C to allow virus
526 binding without internalization. Viral entry was subsequently initiated by shifting cells to 37°C,
527 and cells were fixed at 5 and 20 minutes post-release. TGN46 and H-1PV capsid were
528 detected by immunostaining, and samples were imaged using super-resolution confocal
529 microscopy. In PDAC087T cells overexpressing TGN46, a pronounced accumulation of H-
530 1PV capsid was observed at the cell periphery as early as 5 minutes post-release (Fig. 3C,
531 left panel). At 20 minutes post-release, extensive viral internalization was detected in
532 TGN46-overexpressing cells, with significant co-localization of the viral capsid within TGN46-
533 positive vesicles, consistent with trafficking through TGN-associated compartments (Fig. 3C,
534 right panel). Comparable capsid-TGN46 co-localization was also observed in wild-type
535 PDAC087T cells, although it occurred at later time points (60 minutes post-release) and with
536 reduced TGN46 accumulation (Fig. S2C). Notably, cells in prophase, a stage characterized
537 by fragmentation of the TGN and disruption of vesicular trafficking, displayed an
538 accumulation of TGN46/capsid-positive vesicles (Fig. S2D), consistent with a block at an
539 early stage of viral entry.

540 To determine whether TGN46 interacts with the H-1PV virions at the cell surface prior to
541 internalization, as would be expected for a functional viral receptor, we explored
542 experimental conditions that stabilize TGN46 at the plasma membrane. Owing to its rapid

543 recycling kinetics, visualization of surface-localized TGN46 under steady-state conditions is
544 technically challenging. Previous studies have shown that inhibition of dynamin I impairs the
545 scission of clathrin-coated pits, resulting in the accumulation of TGN46 at the cell surface
546 and a concomitant block in CME[31]. We therefore treated PDAC087T cells with increasing
547 concentrations of hydroxy-dynasore, a reversible, non-competitive inhibitor of dynamin I, to
548 phenocopy this condition. To validate CME inhibition, we monitored uptake of transferrin-
549 Alexa647 (TFn-647) after 5 minutes of incubation and quantified fluorescent intensity and
550 area by immunofluorescence (Fig. S2E-F). As expected, TFn-647 internalization was dose-
551 dependently inhibited by dynasore, with near-complete blockade at 100 μM (-95% ± 1.5%,
552 $p<0.001$, Fig. S2F). In parallel, total TGN46 levels remained unchanged (Fig. S2E and S2G),
553 whereas the spatial distribution of the protein shifted, with a significant increase in
554 membrane-associated signal, consistent with plasma membrane accumulation (3.1-fold ±
555 0.2, $p<0.001$, Fig. S2E and S2H). We next assessed whether surface-localized TGN46
556 engages the H-1PV capsid. PDAC087T-*TGOLN2*-KO cells reconstituted with a doxycycline-
557 inducible *TGOLN2*-GFP construct were used to compare TGN46-high and TGN46-low cells.
558 Cells were pretreated with dynasore or DMSO and exposed to H-1PV under synchronized
559 infection conditions. At defined time points, cells were immunoassayed for H-1PV capsid
560 proteins and either Rab5a (Fig. 3D) or EEA1 (Fig. 3E) to label early endosomes; TGN46-
561 GFP was detected directly via GFP fluorescence. Under control conditions, TGN46-high cells
562 showed greater accumulation of H-1PV capsids compared to TGN46-low cells, with both
563 TGN46 and capsid signals progressively localizing to Rab5a+ and EEA1+ endosomes. In
564 contrast, dynasore treatment prevented internalization, resulting in co-localization of TGN46
565 and capsids at the plasma membrane, without detectable overlap with Rab5a or EEA1 (Fig.
566 S2I). These results indicate that TGN46 engages H-1PV at the cell surface within Rab5a-
567 enriched microdomains prior to CME. Collectively, our data identify TGN46 as a novel entry
568 factor for H-1PV that transiently localizes to the plasma membrane to mediate viral
569 engagement before internalization.

570 **TGN46 domain I interacts with H-1PV capsid proteins for successful infection**. To
571 elucidate the mechanism underlying the interaction between TGN46 and H-1PV, we used
572 AlphaFold 2.0 to predict potential structural interfaces between the lumenal domain of
573 TGN46 and the viral capsid proteins. We submitted the full lumenal sequence of TGN46,
574 which behaves as an intrinsically disordered region (IDR) and is therefore challenging to
575 model, together with the full VP2 sequence, to AlphaFold (Fig. 4A). This analysis generated
576 five models, which were evaluated using the predicted local distance difference test
577 (pLDDT), predicted aligned error (PAE), predicted template modeling score (pTM), and
578 interface pTM (ipTM) (Fig. 4B). As expected, the high flexibility of the IDR resulted in low

579 ipTM values; however, the top-ranked model showed moderate confidence (pLDDT = 62.7,
580 pTM = 0.618, ipTM = 0.212). Notably, all five models converged on a predicted interaction
581 between domain I of TGN46 and the sialic acid (SIA)-binding pocket of VP2 (Fig. 4B). To
582 improve modelling accuracy, we truncated the input sequences to include only the first 50
583 amino acids of TGN46 domain I and the SIA-binding pocket of VP2. This refinement resulted
584 in a marked increase in prediction scores (pLDDT = 87.6, pTM = 0.855, ipTM = 0.372),
585 supporting a higher-confidence interaction model between TGN46 domain I and VP2.

586 To functionally validate these predictions, we conducted TGN46 rescue experiments in
587 PDAC087T *TGOLN2* KO cells. Cells were transduced with lentiviral vectors encoding dox-
588 inducible *TGOLN2* fused to a FLAG tag at either the N- or C-terminus (Fig. S3A). Control
589 conditions included empty vectors or EGFP alone. Truncated versions of TGN46 lacking
590 individual lumenal domains (ΔI, ΔII, ΔIII) were also generated, with the signal peptide
591 preserved. Immunofluorescence confirmed proper expression of all constructs (Fig. S3B).
592 We then assessed the ability of FLAG-tagged TGN46 variants to rescue H-1PV infection in
593 PDAC087T-KO cells. Following H-1PV infection, infectivity was measured by
594 immunofluorescence detection of conformational capsid proteins. C-terminally FLAG-tagged
595 TGN46 fully restored H-1PV infectivity in PDAC087T-KO cells (Fig. 4C). We also generated
596 a C-terminally GFP-tagged version of TGN46, which was validated for proper expression
597 (Fig. S3C) and similarly rescued infection in PDAC087T-KO cells (Fig. S3D). In contrast, N-
598 terminally tagged constructs failed to restore infectivity (Fig. 4C, Fig. S34). Among the
599 domain-deletion mutants, the ΔII and ΔIII variants supported infection at levels comparable to
600 full-length TGN46, whereas the ΔI mutant failed to restore infectivity, indicating that luminal
601 domain I (32 amino acids) is essential for H-1PV infection (Fig. 4C).

602 To assess whether TGN46 physically associates with the H-1PV capsid, we performed GFP-
603 TRAP co-immunoprecipitation assays in PDAC087T-WT cells transduced with EGFP-tagged
604 TGN46 constructs. Following H-1PV infection, GFP fusion proteins were immunoprecipitated
605 using anti-GFP nanobodies (Fig. S3E). Western blot analysis revealed that the viral capsid
606 proteins VP1 and VP2 co-immunoprecipitated specifically with C-terminally tagged TGN46
607 variants, indicating that TGN46 and the H-1PV capsid belong to the same molecular complex
608 (Fig. 4D). Notably, under these conditions, TGN46 did not associate with the viral protein
609 NS1 nor with galectin-1 (Fig. S3H). Domain-deletion analysis showed that TGN46 variants
610 lacking domains II or III retained capsid interaction, whereas deletion of domain I (ΔI)
611 reduced VP1 and VP2 binding by 75% and 65%, respectively (Fig. 4D). Considering the
612 critical role of protein glycosylation in H-1PV infection[14], we investigated the contribution of
613 post-translational modifications in TGN46 and H-1PV interaction. TGN46-EGFP expressing
614 cells were treated with neuraminidase (NA), that cleaves sialic acid residues from

615 glycoproteins and glycolipids on the cell surface. We found that NA treatment significantly
616 inhibited H-1PV entry (- 53% ± 15 %, $p<0.05$, Fig. S3I) and induced a mobility shift of mature
617 TGN46 (Fig. 4D). Importantly, NA treatment decreased co-immunoprecipitation of VP1 and
618 VP2 by 50% and 35%, respectively (Fig. 4D). To further probe the role of glycosylation in
619 TGN46-mediated H-1PV entry, we mutated the sole predicted N-glycosylation site within
620 domain I by at asparagine 39 (N39) to glutamine (Q), a conservative substitution that
621 prevents glycosylation while preserving local structure. This N39Q mutation reduced VP1
622 binding by 35% without affecting VP2 interaction, indicating that this glycosylation contributes
623 to the VP1-TGN46 association (Fig. 4D). Together, these results demonstrate that TGN46
624 binds H-1PV capsid proteins through domain I, and confirms that sialylated glycosylation is
625 an important determinant of this interaction.

626 **TGN46 is a key determinant of H-1PV entry and oncolytic activity in PDAC cells**. Given
627 that mechanistic studies have collectively identified TGN46 as a critical mediator of H-1PV
628 entry, we next examined whether this dependency dictates the specificity and the oncolytic
629 efficacy of H-1PV in PDAC cells. H-1PV entry was quantified across a panel of PDAC-
630 derived cell lines following infection with an MOI of 200 of the virus, using normal pancreatic
631 ductal epithelial (HPDE) cells as a non-malignant control. HPDE cells exhibited remarkably
632 low levels of viral entry ($1.3x10^4$ a.u. ± $0.7x10^4$), which were significantly lower than those
633 observed in Capan-2 ($4x10^4$ a.u. ± $2.7x10^4$, $p < 0.05$), BxPC-3 ($9x10^4$ a.u. ± $2.4x10^4$, $p <$
634 0.0001), Mia PaCa-2 ($1.1x10^5$ a.u. ± $2.3x10^4$, $p < 0.0001$), and Panc-1 cells ($2.2x10^5$ a.u. ±
635 $4.5x10^4$, $p < 0.0001$), the latter showing the highest susceptibility to infection ($p<0.0001$, Fig.
636 5A). In contrast, AsPC-1 cells did not show a significant difference in H-1PV entry compared
637 to HPDE cells ($2.5x10^4$ a.u. ± $0.6x10^4$, $p = 0.4$; Fig. 5A). We then investigated the half-
638 maximal inhibitory concentration (IC_{50}) of H-1PV on the same panel of cells. Normal HPDE
639 exhibited pronounced resistance to H-1PV, with no measurable IC_{50} (Fig. 5B). Among PDAC
640 cells, AsPC-1 (IC_{50} MOI = 193.2 ± 2.3) and Capan-2 (IC_{50} MOI = 132.6 ±2.1) were classified
641 as resistant, while BxPC-3 (IC_{50} MOI = 19.6 ±1.3), Mia PaCa-2 (IC_{50} MOI = 5.4 ±0.7), and
642 Panc-1 (IC_{50} MOI = 2.8 ±0.45) displayed marked susceptibility to viral cytotoxicity. These
643 same cell lines were subsequently analysed for the protein expression of TGN46, along with
644 two known modulators of H-1PV entry, galectin-1[15,32] and laminin subunit gamma-1
645 (LAMC1)[33], to explore potential correlations with viral sensitivity. Interestingly, both galectin-1
646 and LAMC1 were detected in HPDE cells despite their resistance to infection (Fig. S4A).
647 While galectin-1 expression alone showed a positive correlation with H-1PV sensitivity
648 across the panel, LAMC1 levels did not reflect IC_{50} values (Fig. S4A). Remarkably, TGN46
649 expression was absent in HPDE cells and positively correlated with H-1PV sensitivity in
650 PDAC-derived cells (Fig. S4A).

651 To further investigate the contribution of TGN46 to H-1PV infectivity, we deleted *TGOLN2* in
652 highly susceptible, TGN46-positive Panc-1 cells using CRISPR/Cas9. Loss of TGN46
653 expression was confirmed by Western blot (Fig. S4B) and resulted in a 7.5-fold increase in
654 the H-1PV IC_{50} ($p < 0.0001$; Fig. 5C), indicating reduced viral sensitivity. In mirror studies, we
655 conditionally overexpressed TGN46 in TGN46-low, H-1PV resistant AsPC-1 cells. Dox
656 addition successfully induced TGN46 expression (Fig. S4C, $p<0.0001$), and resulted in an a
657 6.2-fold induction of H-1PV entry (Fig. 5D, $p<0.0001$) and significant sensitization to H-1PV
658 infection (+35% ± 8, $p<0.01$, Fig. 5E). We extended our analysis to primary PDAC-derived
659 cultures, as these may better capture tumour heterogeneity than established cell lines and
660 enhance clinical relevance. We quantified H-1PV entry and found that PDAC087T cells
661 exhibited high levels of viral entry (9.7×10^4 a.u. ± 1.3×10^4, $p < 0.0001$; Fig. 5F).
662 Interestingly, these cells expressed the highest protein levels of TGN46 and galectin-1 (Fig.
663 S4D). We then measured the IC_{50} of H-1PV on primary PDAC cells. IC_{50} was not reached for
664 PDAC084T, PDAC072T and PDAC051T cultures, that were classified as resistant, while
665 PDAC091T (IC_{50} MOI = 27.7 ±1.3), PDAC087T (IC_{50} MOI = 8.9 ±0.7), and PDAC012T (IC_{50}
666 MOI = 3.7 ±0.45) were highly susceptible to H-1PV-induced cytotoxic effects. We then
667 applied the same strategy used in established cell lines to assess the role of TGN46 in H-
668 1PV infection of primary cells by deleting *TGOLN2* using CRISPR–Cas9 in susceptible
669 PDAC087T cells. Targeting TGN46 expression resulted in a 19-fold increase in the H-1PV
670 IC_{50} ($p<0.0001$, Fig. 5H), corresponding to reduced sensitivity to viral infection. Importantly,
671 these results extend our findings from cell lines to primary PDAC cultures and demonstrate
672 that TGN46 contributes not only to H-1PV infection but also to its oncolytic activity. Together,
673 these data warrant further exploration of TGN46 function in experimental models *in vivo*.

674 **TGN46 is required for H-1PV antitumoral activity *in vivo***

675 To assess the contribution of TGN46 to H-1PV oncolytic activity *in vivo*, we generated
676 subcutaneous tumors from primary PDAC087T cells in which *TGOLN2* was deleted using
677 CRISPR-Cas9 (Fig. 6A). Efficient and sustained depletion of *TGOLN2* in tumour tissues was
678 confirmed at the protein level by Western blot analysis (Fig.6B). Following two intratumoral
679 administrations of H-1PV, control tumours exhibited a marked reduction in tumour volume
680 ($321.5mm^3 \pm 15.9$ vs $160mm^3 \pm 27.9$, $p<0.01$) and weight ($0.3g \pm 0.04$ vs $0.18g \pm 0.02$, $p<0.05$),
681 consistent with robust oncolytic activity, compared to control mice receiving PBS (Fig. 6C
682 and 6D). In contrast, *TGOLN2*-deficient tumours failed to respond to H-1PV treatment,
683 showing no significant reduction in tumour volume or mass (Fig. 6E and 6F). Consistent with
684 this loss of therapeutic efficacy, quantification of viral genomes at the experimental endpoint
685 revealed a significant decrease in H-1PV copy number in *TGOLN2*-depleted tumors
686 compared with controls ($4.1x10^3$a.u.$\pm 1.7x10^3$ vs $0.3x10^3$a.u.$\pm 0.1x10^3$, $p<0.05$, Fig. 6G).

687 Collectively, these results demonstrate that TGN46 expression is required for productive H-
688 1PV infection and oncolytic activity in experimental PDAC tumour models.

689

690 **Discussion**

691 Oncolytic viruses offer a promising approach to selectively target malignant cells while
692 sparing normal tissues[4]. Among these, H-1PV stands out due to its non-pathogenicity in
693 humans, its natural oncotropism and safety in clinical trials[8,9,10]. However, the molecular basis
694 of this selectivity has remained partly defined. Contrary to many OV, the oncoselectivity of
695 parvoviruses in human cells does not appear to rely on impaired innate immunity within
696 cancer cells. Studies have demonstrated that IFN signalling fails to reduce H-1PV infectivity
697 or progeny production in both normal and transformed cells[34,35], despite the upregulation of
698 interferon-stimulated genes (ISGs)[35]. This unexpected resistance to IFN-mediated antiviral
699 responses may stem from either the absence of functional pattern recognition receptor
700 (PRR) expression or intrinsic defects, potentially virus-driven, in the endosomal sensing of
701 parvoviral genomes[36]. Notably, H-1PV susceptibility does not correlate with absolute ISG
702 levels but rather with the efficiency of viral entry. This is exemplified by the cooperative role
703 of laminin γ1[33] and galectin-1[15], the later recently confirmed as a key mediator of H-1PV
704 efficacy during a biomarker screen in PDAC cell cultures[32].Yet, despite that H-1PV efficacy in
705 PDAC appears to rely almost entirely on effective cell entry, the identity of high-affinity cell
706 surface receptors facilitating H-1PV uptake has remained elusive, and definitive biomarkers
707 predicting viral susceptibility remains to be fully established.

708 In this study, we demonstrate that TGN46 is involved early stages of viral entry, supports
709 productive infection, and is required for downstream oncolytic activity. TGN46 is encoded by
710 *TGOLN2* and is widely expressed across various human tissues, particularly in epithelial and
711 secretory cells, where it plays a role in protein sorting and trafficking within the TGN. It
712 functions as a cargo receptor, facilitating the sorting of secretory proteins into specific
713 vesicles for delivery to their destinations[37]. There is no direct link between TGN46 and
714 cancer, but it has been implicated in the formation of CARTS (carriers of the TGN to the cell
715 surface), a PKD-dependent pathway critical for the secretion of specific cargo[38], particularly
716 that of pancreatic adenocarcinoma upregulated factor (PAUF)[39], that is associated with
717 TGFβ-dependent increase in the migration and invasion of PDAC cell lines[40], and possibly in
718 the establishment of an immunosuppressive tumor microenvironment[41].

719 Using for the first time in the filed a combination of genetic perturbation, high-resolution
720 imaging, co-immunoprecipitation, and functional virological assays, we demonstrate that
721 TGN46 transiently localizes to the plasma membrane where it engages the H-1PV capsids in
722 Rab5a-enriched domains, prior to CME. This previously underestimated surface function of
723 TGN46 contrasts with the aforementioned classical role as a resident of the TGN, revealing
724 new insights into the dynamic trafficking of this protein and its potential repurposing in the
725 context of viral entry. This echo recent findings indicating that TGN46 plays a role in the

726 intracellular trafficking of SARS-CoV-2 proteins, especially SARS-CoV-2 E protein that
727 undergoes retrograde trafficking to the TGN, accumulating in LAMP1-positive vesicles, likely
728 lysosomes[42].

729 Our findings position TGN46 as a *bona fide* host factor for H-1PV infection in PDAC cells and
730 TGN46 and H-1PV virions colocalize at the cell membrane. Mechanistically, TGN46 domain I
731 emerges as both necessary and sufficient for H-1PV internalization following interaction with
732 H-1PV capsid proteins, whereas domains II and III were dispensable. Treatment with
733 sialylation inhibitor neuraminidase or mutation of the single predicted glycosylation site within
734 domain I (N39) impaired binding to VP1 but not VP2, suggesting distinct roles for glycan-
735 mediated interactions in capsid recognition. Interestingly, TGN46 does not bind with the non-
736 structural NS1 protein or galectin-1 itself, suggesting that TGN46 may act as a primary
737 attachment or internalization factor rather than a broader viral scaffold. Despite the strength
738 of these findings, our study has several limitations. First, while we have established a
739 physical association between TGN46 and the H-1PV capsid, the precise molecular interface
740 remains undefined. Structural studies, such as cryo-EM or crosslinking-mass spectrometry,
741 could help map the interaction site and guide rational design of virus mutants with improved
742 binding properties. Second, although TGN46 appears to be expressed and localized to the
743 plasma membrane in PDAC cells, the underlying regulation of expression or trafficking
744 mechanisms are unknown. Future work should determine whether this pattern of expression
745 and localization is driven by oncogenic signalling pathways or specific post-translational
746 modifications, and whether it is unique to PDAC or observed in other H-1PV-sensitive
747 tumors.

748 Furthermore, our study uncovers several key insights with significant translational potential.
749 First, we quantified H-1PV infection efficiency across a panel of established PDAC cell lines
750 and primary patient-derived tumor cells. Susceptibility varied markedly, with some cell lines
751 showing robust infection and others remaining refractory. Second, we show that TGN46
752 expression correlates with susceptibility to H-1PV across both cell lines and patient-derived
753 samples. Third, functional studies demonstrate that inducible overexpression of TGN46 in
754 otherwise resistant cells restored susceptibility to infection. In contrast, CRISPR-mediated
755 deletion of *TGOLN2* strongly attenuated viral infectivity and efficacy, both *in vitro* and *in vivo*
756 in experimental tumor models. These data not only validate TGN46 as a host factor for H-
757 1PV, but also indicate that its expression level is rate-limiting for virotherapy efficacy.
758 Collectively, our findings suggest that TGN46 may serve as predictive biomarker of H-1PV
759 responsiveness in PDAC, a notoriously heterogeneous and treatment-refractory malignancy.
760 The ability to stratify PDAC based on TGN46 expression could offer a biomarker-based
761 approach to personalize oncolytic virus therapies. Pre-treatment screening could help identify

762 patients most likely to benefit from virotherapy. Moreover, our data raise the possibility of
763 pharmacologically enhancing TGN46 expression or surface localization to sensitize
764 otherwise refractory tumors. In conclusion, this study reveals an unexpected role for TGN46
765 in mediating H-1PV entry and positions this protein as a critical determinant of virotherapy
766 responsiveness in PDAC. These insights pave the way for refined biomarker-driven
767 approaches and underscore the value of probing unconventional host-virus interactions in
768 the development of targeted cancer therapeutics.

769

770

771 **Figure legends**

772

773 **Figure 1: CRISPR/Cas9 KO screen identifies TGOLN2 as a host gene for H-1PV**
774 **infection. A.** CRISPR/Cas9 KO screening strategy of H-1PV host genes. PDAC087T cells
775 constitutively expressing Cas9 nuclease enzyme were transduced with the lentiviral pooled
776 sgRNA library GeckoV2 at 0.3 MOI to obtain one gene KO per cell. Cells were then infected
777 with H-1PV or not (NI) at a MOI of 10 and sgRNA content of each population was determined
778 by PCR of sgRNA locus, NGS sequencing and MAGeCK sgRNA enrichment analysis. **B.**
779 Micrograph showing each individual gene screened with an arbitrary gene number in x-axis
780 and the sgRNA positive enrichment score determined with MAGeCK algorithm in y-axis.
781 Genes under positive enrichment score cut-off are drawn with gray dots; genes above cut-off
782 were annotated and grouped by family: sialic acid metabolism (yellow dots), vesicular
783 trafficking / protein secretion (orange dots) and others (teal dots). **C.** Representative
784 validation of gRNA screening results. Examples are shown for control non-targeting gRNAs,
785 for non-validated gRNAs that did not affect viral cytotoxicity (targeting *MSLN*, *CORO7*), and
786 for validated gRNAs that abolished viral lytic activity (targeting *UNC50*, *TGOLN2*). An MOI of
787 5 was used for H-1PV infection. Cell confluence was monitored using the IncuCyte live-cell
788 imaging system. Data represent the mean ± S.D. of three independent biological
789 experiments performed in triplicate. **D.** Individual validation of genes above positive
790 enrichment score threshold. PDAC087T-Cas9 cells were transduced to express stably
791 individual sgRNAs of each gene to validate (2 sgRNA per gene and 3 non-targeting human
792 control sgRNAs), then cells were infected or not with H-1PV at MOI 5. 48h post infection, cell
793 viability assay was performed and survival ratio (infected / NI) calculated for each sgRNA.
794 Mean ratios of the three non-targeting human controls sgRNA were pooled (P, red dots) and
795 use as reference to calculate resistance to H-1PV conferred by each individually tested
796 sgRNA (% variation of infected / NI). Negative value stands for increased sensitivity to
797 infection. Dots and bars colors correspond to target gene family: non-targeting (gray and light
798 gray), sialic acid metabolism (yellow), vesicular trafficking (orange) and others (blue). For
799 statistical analysis, Fisher's LSD multiple comparisons test was performed.

800

801 **Figure 2: H-1PV rely on TGN46 expression for successful infection and oncolytic**
802 **activity.** (**A, F**) cell counts, (**B, G**) intracellular H-1PV viral genomes content (qPCR targeting
803 the NS1 genomic locus) and (**C, H**) H-1PV viral genomes in the supernatant of PDAC087T-
804 WT and *TGOLN2*-KO cells (**A-C**), and control or of TGN46-overexpressing PDAC087T cells
805 (**F-H**), measured 48h post H-1PV infection. Infections were performed at MOI 2.5 and 10.
806 Statistical comparisons were performed using a two-way ANOVA. (D, E)

807 Immunofluorescence (IF) analysis of PDAC087T-WT and *TGOLN2*-KO cells, and (I, J)
808 control or TGN46-overexpressing PDAC087T cells, 24 h post–H-1PV infection at an MOI of
809 2.5. Cells were stained with anti-TGN46 antibody (green) and DAPI for DNA counterstaining
810 (light gray). Anti-NS1 antibody (orange) and anti-H-1PV conformational capsid antibody (red)
811 were used to detect viral proteins. Images were acquired using a wide-field microscope with
812 a 20X objective (scale bars: 100 µm).

813

814 **Figure 3: Modifications in TGN46 expression level do not impact CME but controls H-**
815 **1PV entry.** PDAC087T-WT (WT) cells, or PDAC087T cells KO for *TGOLN2* (KO-T, **A**), and
816 PDAC087T cells overexpressing (+) or not (-) TGN46 (**B**) were infected with H-1PV at MOI
817 2.5 and incubated 15, 60, 120 or 240 min at 37°C followed with extensive wash with PBS, to
818 remove unbound virus, and internalized viral genomes were quantified by qPCR against NS1
819 genomic locus**.** Statistical comparisons were performed using a two-way ANOVA**. C.** Cells
820 were pre-incubated for 15 min at 4°C and then infected with H-1PV at an MOI of 250 for 1 h
821 at 4°C to allow viral binding to the cell surface. Cells were subsequently shifted to 37°C for 5
822 or 20 min, extensively washed with PBS, fixed, and processed for IF staining of TGN46
823 (green), viral capsid (red), and DAPI for DNA counterstaining (light gray). Images were
824 acquired using a confocal microscope with a 63× objective (scale bars, 20 µm). Regions of
825 interest were magnified 5-fold. PDAC087T-*TGOLN2*-KO cells reconstituted with a
826 doxycycline-inducible TGN46-GFP construct and pretreated for 30 min with DMSO (control,
827 **D** and **E**, left panels) or 100µM hydroxy-dynasore (Dyn, **D** and **E**, right panels). Cells were
828 infected with H-1PV at an MOI of 250 for the indicated times, and stained with antibodies
829 against TGN46 and viral capsids (D, E), together with antibodies against Rab5a (**D**) or EEA1
830 (**E**) and DAPI for DNA counterstaining (light gray)**.** Images were acquired using a confocal
831 microscope with a 63× objective (scale bars, 20 µm).

832

833 **Figure 4: H-1PV infection requires interaction of capsid proteins with sialic acid motifs**
834 **present in TGN46 N-terminal domain I. A**. Predicted model of the interaction between the
835 full luminal domain of TGN46 and H-1PV capsid proteins generated using AlphaFold 2.0. **B**.
836 Model evaluation based on predicted local distance difference test (pLDDT), predicted
837 aligned error (PAE), predicted template modeling score (pTM), and interface predicted
838 template modeling score (ipTM). **C.** PDAC087T-WT cells (gray bars); PDAC087T cells with
839 dox-inducible TGN46 expression (orange bars), PDAC087T-*TGOLN2*-KO cells (green bars);
840 and PDAC087T-*TGOLN2*-KO cells co-expressing dox-inducible FLAG-TGN46, TGN46-
841 FLAG, TGN46ΔI-FLAG, TGN46ΔII-FLAG, or TGN46ΔIII-FLAG (pink bars) were treated with

842 0, 50, or 500 µg/mL dox) and infected with H-1PV at an MOI of 2.5 for 24 h. Cells were fixed
843 and stained with an antibody against H-1PV conformational capsid proteins and DAPI for
844 DNA counterstaining (light gray). Images were acquired using a confocal microscope with a
845 20× objective. Total capsid fluorescence intensity per cell was quantified and normalized to
846 the control condition (red dotted line). Data represent mean ± SD of three independent
847 experiments performed in triplicate. Statistical analysis was performed using uncorrected
848 Fisher's LSD test**. D.** PDAC087T-*TGOLN2*-KO cells transduced with lentiviral vectors
849 encoding EGFP, EGFP-TGN46, TGN46-EGFP, TGN46ΔI-EGFP, TGN46ΔII-EGFP,
850 TGN46ΔIII-EGFP, or TGN46N39Q-EGFP were infected with H-1PV at an MOI of 2.5. In
851 addition, PDAC087T-*TGOLN2*-KO cells expressing TGN46-EGFP were treated with
852 neuraminidase prior to infection. Two days post-infection, cellular proteins were extracted
853 and incubated with GFP-Trap beads. Bead-bound proteins were resolved by western blot.
854 Input whole-cell lysates and GFP-Trap co-immunoprecipitated proteins were analyzed by
855 western blot for EGFP, VP1, and VP2.

856

857 **Figure 5: TGN46 drives H-1PV entry and oncolytic efficacy in pancreatic ductal**
858 **adenocarcinoma cells. A**. PDAC cell lines were infected with H-1PV (MOI 200) for 2 hours.
859 Cells were then fixed and stained with an antibody targeting the conformational H-1PV
860 capsid protein. Normal pancreatic ductal epithelial (HPDE) cells were used as control.
861 Images were acquired using a confocal microscope (63× objective), and fluorescence
862 intensity was quantified. Data represent the mean ± SD of three independent experiments,
863 each performed in triplicate. Statistical comparisons were performed using a two-way
864 ANOVA. **B**. PDAC cell lines were infected with H-1PV at the indicated MOIs. After 48 hours,
865 cell viability was measured using the CellTiter-Glo (CTG) assay, and IC_{50} values were
866 calculated. Data represent the mean ± SD of three independent experiments, each
867 performed in triplicate. **C**. Panc-1 cells with *TGOLN2* knockout were generated using
868 CRISPR/Cas9 and infected with H-1PV at the indicated MOIs. After 48 hours, cell viability
869 was measured using CTG assay. Data represent the mean ± SD of three independent
870 experiments, each performed in triplicate. Statistical comparisons were performed using an
871 unpaired t-test. Lentiviral vectors encoding for TGN46 were used to generate AsPC-1 TGN46
872 cells. Proteins expression was induced or not by doxycycline and cells infected with H-1PV at
873 an MOI of 200 for 2 h (**D**). Cells were then fixed and stained with an antibody targeting the
874 conformational H-1PV capsid protein. Images were acquired using a confocal microscope
875 (63× objective), and fluorescence intensity was quantified. Alternatively, AsPC-1 cells
876 expressing or not TGN46 were infected with H-1PV at an MOI of 50. **E.** After 48 hours, cell
877 viability was measured using the CTG assay. Data represent the mean ± SD of three

878 independent experiments, each performed in triplicate. Statistical comparisons were
879 performed using an unpaired t test. **F.** PDAC primary cells were infected with H-1PV (MOI
880 200) for 2 hours. Cells were then fixed and stained with an antibody targeting the
881 conformational H-1PV capsid protein. Images were acquired using a confocal microscope
882 (63× objective), and fluorescence intensity was quantified. Data represent the mean ± SD of
883 three independent experiments, each performed in triplicate. Statistical comparisons were
884 performed using a two-way ANOVA. **G**. PDAC primary cells were infected with H-1PV at the
885 indicated MOIs. After 48 hours, cell viability was measured using the CTG assay, and IC_{50}
886 values were calculated. Data represent the mean ± SD of three independent experiments,
887 each performed in triplicate. **H**. PDAC087T primary cells with *TGOLN2* knockout were
888 generated using CRISPR/Cas9 and infected with H-1PV at the indicated MOIs. After 48
889 hours, cell viability was measured using CTG assay. Data represent the mean ± SD of three
890 independent experiments, each performed in triplicate. Statistical comparisons were
891 performed using an unpaired t-test.

892

893 **Figure 6: H-1PV antitumoral effects in vivo depend on TGN46. A**. Schematic
894 representation of the in vivo study. PDAC087T-WT or PDAC087T-*TGOLN2*-KO cells were
895 implanted subcutaneously in NSG mice. Eleven days later, experimental tumors received a
896 first intratumoral (IT) injection of 5×10^6 plaque-forming units (p.f.u.) of the virus, followed by
897 a second injection 4 days later. Control mice received two intratumoral injections of PBS.
898 Tumors were sampled and analyzed 7 days after the second viral injection, and TGN46
899 expression was assessed by Western blot (**B**). Tumor volume (**C**, **E**), weight (panels **D**, **F**),
900 were measured, and viral content was quantified by NS1 qPCR (**G**). Data represent the
901 mean ± SD of at least 4-6 animals per group. Statistical comparisons were performed using
902 an unpaired t-test.

903

904 **Figure S1. A.** Schematic representation of the all-in-one plasmid used for CRISPR/Cas9-
905 mediated knockout (KO) of TGN46 (*TGOLN2* sgRNA) by transient transfection followed by
906 ouabain selection. **B.** Western blot analysis of TGN46 expression in PDAC087T-WT and
907 PDAC087T-*TGOLN2*-KO cells. GAPDH was used as loading control. **C.**
908 Immunofluorescence (IF) analysis of PDAC087T-WT (WT) and PDAC087T-*TGOLN2*-KO
909 (KO) cells stained with anti-TGN46 antibody (green) and DAPI for DNA counterstaining (light
910 grey). Images were acquired using a confocal microscope at 63x objective (top row, 20µm
911 scale bars) and regions of interest were magnified 5 times (bottom row). **D.** Western blot
912 analysis of TGN46 expression in Hela cells, and Hela cells expressing *TGOLN2* sgRNA.

913 GAPDH was used as loading control. **E.** Cell viability assay of Hela cells expressing control
914 sgRNA and wild-type for *TGNOL2* (WT), and *TGOLN2*-KO Hela cells (KO) following infection
915 with H-1PV at the indicated MOI. Data represent mean ± S.D. of three independent
916 experiments performed in triplicates. IF analysis of NS1 **(F)** or capsid **(G)** proteins in
917 PDAC087T-WT (WT) and PDAC087T- *TGOLN2*-KO (KO) cells following infection with H-1PV
918 at an MOI of 2.5. Data represent mean ± S.D. of three independent experiments performed
919 in triplicate. Unpaired t-test were performed for statistical analysis. **H.** Schematic
920 representation of all-in-one "pTRE-TGN46" Tet-on lentiviral vector for doxycycline inducible
921 TGN46 overexpression. **I.** Western blot analysis of TGN46 expression in PDAC087T-pTRE-
922 TGN46 cells -/+ dox (TGN46 -/+). HSP90 was used as loading control. **J.** IF of PDAC087T
923 without dox (TGN46 -) and PDAC087T cells overexpressing TGN46 upon dox treatment
924 (TGN46 +), stained with anti-TGN46 antibody (green) and DAPI (light grey). Images were
925 acquired using a confocal microscope at 63X objective (first row, 20µm scale bars) and
926 regions of interest were magnified 5 times. IF analysis of NS1 **(K)** or capsid **(L)** proteins in
927 PDAC087T cells without dox (TGN46 -) and PDAC087T cells overexpressing TGN46 upon
928 dox treatment (TGN46 +), following infection with H-1PV at an MOI of 2.5. Data represent
929 mean ± S.D. of three independent experiments performed in triplicate. Unpaired t-test were
930 performed for statistical analysis.

931

932 **Figure S2. A.** PDAC087T-WT (WT) and PDAC087T-*TGOLN2*-KO (KO) cells, and **(B)**
933 PDAC087T cells without doxycycline (TGN46 −) and PDAC087T cells overexpressing
934 TGN46 upon doxycycline treatment (TGN46 +) were stained with antibodies against
935 vesicular transport-related proteins (CHC, Rab5, EEA1, and LAMP1) or analyzed for TFn-
936 647 uptake. Each row shows representative images of staining for one protein of interest
937 (green) or the TFn-647 signal (pink), along with DAPI counterstaining of DNA (light gray).
938 Images were acquired using a confocal microscope with a 63X objective (scale bars: 20 µm).
939 Quantification of total fluorescence intensity, number of objects, and mean object size (µm²)
940 was performed in 30–50 individual cells per condition. Statistical comparisons were
941 conducted using unpaired t tests. PDAC087T-WT cells in interphase **(C)** or prophase **(D)**
942 were stained with antibodies against TGN46 (green) and viral capsids (red), along with DAPI
943 counterstaining of DNA (light gray). Images were acquired using a confocal microscope with
944 a 63× objective (scale bars: 20 µm). PDAC087T-WT cells were treated with hydroxy-
945 dynasore (Dyn) at the indicated concentrations and stained with antibodies against TGN46
946 (green) or analyzed for TFn-647 uptake (pink), along with DAPI counterstaining of DNA (light
947 gray). **E.** Images were acquired using a confocal microscope with a 20X objective.
948 Transferrin uptake **(F),** TGN46 fluorescence intensity **(G)** and total TGN46-positive area **(H)**

949 were quantified. Data represent mean ± S.D. of three independent experiments performed in
950 triplicate. Šídák's multiple comparisons test were performed for statistical comparisons. **I.**
951 Representative image and signal quantification showing colocalization of TGN46 (green) and
952 viral capsid (red).

953 **Figure S3. A.** Schematic representation of TGN46 fusion proteins (FLAG or GFP in N-or C-
954 terminal, red box) and deleted variants (domain I, II or III, doted lines) generated for rescue
955 and GFP-TRAP experiments (subcloning in previously described pTRE inducible lentivector).
956 Legends: signal peptide (SP), luminal part (Lum.), cytoplasmic part (Cyto.) and
957 transmembrane domain (IV). **B.** PDAC087T-WT cells, or PDAC087T-*TGOLN2*-KO cells were
958 transduced with empty control lentiviral vectos (pTRE) or lentivial vectors encoding for
959 TGN46, FLAG-TGN46 and FLAG-TGN46 domain I, II or III deleted mutants. Protein
960 expression was induced by doxycycline (dox), and cells were stained with antibodies against
961 FLAG and fluorescence was quantified. Data represent mean of three independent
962 experiments performed in triplicate**.** Statistical comparisons were performed using a two-way
963 ANOVA. **C**. PDAC087T-WT cells, or PDAC087T-*TGOLN2*-KO cells were transduced with
964 empty control lentiviral vectos (pTRE) or lentivial vectors encoding for TGN46, EGFP, EGFP-
965 TGN46 and TGN46-EGFP. Proteins expression was induced by doxycycline (dox), and
966 EGFP fluorescence was quantified. Data represent mean of three independent experiments
967 performed in triplicate**.** Statistical comparisons were performed using a two-way ANOVA. **D**.
968 PDAC087T-WT cells, or PDAC087T-*TGOLN2*-KO cells were transduced with empty control
969 lentiviral vectos (pTRE) or lentivial vectors encoding for TGN46, EGFP, EGFP-TGN46 and
970 TGN46-EGFP. Proteins expression was induced by doxycycline (dox) and infected with H-
971 1PV at an MOI of 2.5 for 24 h. Cells were fixed and stained with an antibody against H-1PV
972 conformational capsid proteins and DAPI for DNA counterstaining (light gray). Images were
973 acquired using a confocal microscope with a 20X objective. Total capsid fluorescence
974 intensity per cell was quantified and normalized to the control condition (red dotted line).
975 Data represent mean ± SD of three independent experiments performed in triplicate.
976 Statistical analysis was performed using uncorrected Fisher's LSD test. **E**. Schematic
977 representation of the GFP-Trap strategy. F. PDAC087T-*TGOLN2*-KO cells transduced with
978 lentiviral vectors encoding EGFP, EGFP-TGN46, or TGN46-EGFP were infected with H-1PV
979 at an MOI of 2.5. Two days post-infection, cellular proteins were extracted and incubated
980 with GFP-Trap beads. Input, flowthrough and bead-bound proteins were resolved by western
981 blot for EGFP, VP1, VP2, NS1, GAPDH, and galectin-1 (Gal-1). I, input; FT, flowthrough; B,
982 bead-bound fraction. **F**. PDAC087T cells were pre-treated with neuraminidase, then infected
983 with H-1PV at an MOI of 250. Six hours post-infection, cells were fixed and stained with an
984 antibody against the conformational H-1PV capsid protein. Images were acquired using a

985 confocal microscope with a 63X objective, and fluorescence intensity was quantified. Data
986 represent mean ± SD of three independent experiments performed in triplicate. Statistical
987 comparisons were performed using an unpaired t test.

988 **Figure S4**. **A**. Western blot analysis of TGN46, galectin-1 (Gal-1), and laminin-γ1 expression
989 in the indicated PDAC-derived cell lines. GAPDH was used as a loading control. Data are
990 representative of three independent experiments. **B**. Western blot analysis of TGN46
991 expression in wild-type Panc-1 cells (non-targeting control) and Panc-1 cells expressing
992 *TGOLN2* sgRNA. GAPDH was used as a loading control. Data are representative of three
993 independent experiments. **C**. Immunofluorescence analysis of TGN46 expression in AsPC-1
994 cells either overexpressing (+) or not (–) TGN46. Data represent the mean ± SD of three
995 independent experiments, each performed in triplicate. Statistical comparisons were
996 performed using an unpaired t-test. **D**. Western blot analysis of TGN46 and galectin-1 (Gal-1)
997 expression in the indicated PDAC-derived primary cells. β-actin was used as a loading
998 control. Data are representative of three independent experiments.

999

1000 **References**

1001

1002 1. Wood, L. D., Canto, M. I., Jaffee, E. M. & Simeone, D. M. Pancreatic Cancer: Pathogenesis,
1003 Screening, Diagnosis, and Treatment. *Gastroenterology* **163**, 386-402.e1 (2022).
1004 2. Park, W., Chawla, A. & O'Reilly, E. M. Pancreatic Cancer: A Review. *JAMA* **326**, 851–862 (2021).
1005 3. Halbrook, C. J., Lyssiotis, C. A., Pasca di Magliano, M. & Maitra, A. Pancreatic cancer: Advances
1006 and challenges. *Cell* **186**, 1729–1754 (2023).
1007 4. Kollmann, C. F., van Montfoort, N., Cordelier, P., Pol, J. & Olagnier, D. Oncolytic virotherapy:
1008 Sparking durable anti-tumor immunity through microenvironment modulation. *Semin Immunol*
1009 **80**, 101994 (2025).
1010 5. Zhang, T. *et al.* Talimogene Laherparepvec (T-VEC): A Review of the Recent Advances in Cancer
1011 Therapy. *J Clin Med* **12**, 1098 (2023).
1012 6. Quillien, L., Buscail, L. & Cordelier, P. Pancreatic Cancer Cell and Gene Biotherapies: Past,
1013 Present, and Future. *Hum Gene Ther* **34**, 150–161 (2023).
1014 7. Runcie, K. *et al.* Phase I study of intratumoral injection of talimogene laherparepvec for the
1015 treatment of advanced pancreatic cancer. *Oncologist* oyae200 (2024)
1016 doi:10.1093/oncolo/oyae200.
1017 8. Angelova, A. L., Geletneky, K., Nüesch, J. P. F. & Rommelaere, J. Tumor Selectivity of Oncolytic
1018 Parvoviruses: From in vitro and Animal Models to Cancer Patients. *Frontiers in Bioengineering*
1019 *and Biotechnology* **3**, (2015).
1020 9. Geletneky, K. *et al.* Oncolytic H-1 Parvovirus Shows Safety and Signs of Immunogenic Activity in a
1021 First Phase I/IIa Glioblastoma Trial. *Molecular Therapy* **25**, 2620–2634 (2017).
1022 10. Hajda, J. *et al.* A non-controlled, single arm, open label, phase II study of intravenous and
1023 intratumoral administration of ParvOryx in patients with metastatic, inoperable pancreatic
1024 cancer: ParvOryx02 protocol. *BMC Cancer* **17**, 1–11 (2017).

1025 11. Hajda, J. *et al.* Phase 2 Trial of Oncolytic H-1 Parvovirus Therapy Shows Safety and Signs of
1026 Immune System Activation in Patients With Metastatic Pancreatic Ductal Adenocarcinoma.
1027 *Clinical Cancer Research* **27**, 5546–5556 (2021).
1028 12. Bretscher, C. & Marchini, A. H-1 Parvovirus as a Cancer-Killing Agent: Past, Present, and Future.
1029 *Viruses* **11**, 562 (2019).
1030 13. Hristov, G. *et al.* Through Its Nonstructural Protein NS1, Parvovirus H-1 Induces Apoptosis via
1031 Accumulation of Reactive Oxygen Species. *Journal of Virology* **84**, 5909–5922 (2010).
1032 14. Kulkarni, A. *et al.* Oncolytic H-1 parvovirus binds to sialic acid on laminins for cell attachment and
1033 entry. *Nat Commun* **12**, 3834 (2021).
1034 15. Ferreira, T. *et al.* Oncolytic H-1 Parvovirus Hijacks Galectin-1 to Enter Cancer Cells. *Viruses* **14**,
1035 1018 (2022).
1036 16. Vasta, G. R. Roles of galectins in infection. *Nat Rev Microbiol* **7**, 424–438 (2009).
1037 17. Ferreira, T. *et al.* Oncolytic H-1 Parvovirus Enters Cancer Cells through Clathrin-Mediated
1038 Endocytosis. *Viruses* **12**, 1199 (2020).
1039 18. Ferreira, T. *et al.* Oncolytic H-1 Parvovirus Enters Cancer Cells through Clathrin-Mediated
1040 Endocytosis. *Viruses* **12**, 1199 (2020).
1041 19. Toolan, H. W., Dalldore, G., Barclay, M., Chandra, S. & Moore, A. E. An unidentified, filtrable
1042 agent isolated from transplanted human tumors*. *Proceedings of the National Academy of*
1043 *Sciences* **46**, 1256–1258 (1960).
1044 20. Lujan, P. *et al.* Sorting of secretory proteins at the trans-Golgi network by TGN46. *eLife* **12**,
1045 (2023).
1046 21. Fraunhoffer, N. A. *et al.* Evidencing a Pancreatic Ductal Adenocarcinoma Subpopulation Sensitive
1047 to the Proteasome Inhibitor Carfilzomib. *Clin Cancer Res* **26**, 5506–5519 (2020).
1048 22. Angelova, A. L. *et al.* Complementary induction of immunogenic cell death by oncolytic
1049 parvovirus H-1PV and gemcitabine in pancreatic cancer. *J. Virol.* **88**, 5263–5276 (2014).

1050 23. Joung, J. *et al.* Genome-scale CRISPR-Cas9 knockout and transcriptional activation screening.
1051 *Nature Protocols* **12**, 828–863 (2017).
1052 24. Li, W. *et al.* MAGeCK enables robust identification of essential genes from genome-scale
1053 CRISPR/Cas9 knockout screens. *Genome Biology* **15**, 554 (2014).
1054 25. Agudelo, D. *et al.* Marker-free coselection for CRISPR-driven genome editing in human cells.
1055 *Nature Methods* **14**, 615–620 (2017).
1056 26. Tessmer, C. *et al.* Generation and Validation of Monoclonal Antibodies Suitable for Detecting and
1057 Monitoring Parvovirus Infections. *Pathogens* **11**, 208 (2022).
1058 27. Liu, X. *et al.* An AP-MS- and BioID-compatible MAC-tag enables comprehensive mapping of
1059 protein interactions and subcellular localizations. *Nat Commun* **9**, 1188 (2018).
1060 28. Zhuo, C. *et al.* Spatiotemporal control of CRISPR/Cas9 gene editing. *Signal Transduct Target Ther*
1061 **6**, 238 (2021).
1062 29. Li, J. *et al.* Synergistic combination of valproic acid and oncolytic parvovirus H-1PV as a potential
1063 therapy against cervical and pancreatic carcinomas. *EMBO Mol Med* **5**, 1537–1555 (2013).
1064 30. Mayle, K. M., Le, A. M. & Kamei, D. T. The intracellular trafficking pathway of transferrin. *Biochim*
1065 *Biophys Acta* **1820**, 264–281 (2012).
1066 31. Banting, G., Maile, R. & Roquemore, E. P. The steady state distribution of humTGN46 is not
1067 significantly altered in cells defective in clathrin-mediated endocytosis. *J Cell Sci* **111 (Pt 23)**,
1068 3451–3458 (1998).
1069 32. Schäfer, T. E. *et al.* Biomarker screen for efficacy of oncolytic virotherapy in patient-derived
1070 pancreatic cancer cultures. *EBioMedicine* **105**, 105219 (2024).
1071 33. Kulkarni, A. *et al.* Oncolytic H-1 parvovirus binds to sialic acid on laminins for cell attachment and
1072 entry. *Nat Commun* **12**, 3834 (2021).
1073 34. Paglino, J. C., Andres, W. & van den Pol, A. N. Autonomous parvoviruses neither stimulate nor
1074 are inhibited by the type I interferon response in human normal or cancer cells. *J Virol* **88**, 4932–
1075 4942 (2014).

1076 35. Neulinger-Muñoz, M. *et al.* Human Retrotransposons and the Global Shutdown of Homeostatic
1077 Innate Immunity by Oncolytic Parvovirus H-1PV in Pancreatic Cancer. *Viruses* **13**, 1019 (2021).
1078 36. Raykov, Z. *et al.* TLR-9 contributes to the antiviral innate immune sensing of rodent parvoviruses
1079 MVMp and H-1PV by normal human immune cells. *PLoS One* **8**, e55086 (2013).
1080 37. Lujan, P. *et al.* Sorting of secretory proteins at the trans-Golgi network by human TGN46. *eLife*
1081 **12**, RP91708 (2024).
1082 38. Wakana, Y. *et al.* Kinesin-5/Eg5 is important for transport of CARTS from the trans-Golgi network
1083 to the cell surface. *Journal of Cell Biology* **202**, 241–250 (2013).
1084 39. Wakana, Y. *et al.* A new class of carriers that transport selective cargo from the trans Golgi
1085 network to the cell surface. *The EMBO Journal* **31**, 3976–3990 (2012).
1086 40. Lee, M. *et al.* TGF-β-Induced PAUF Plays a Pivotal Role in the Migration and Invasion of Human
1087 Pancreatic Ductal Adenocarcinoma Cell Line Panc-1. *Int J Mol Sci* **25**, 11420 (2024).
1088 41. Kim, Y. J. *et al.* Pancreatic Adenocarcinoma Up-Regulated Factor (PAUF) Transforms Human
1089 Monocytes into Alternative M2 Macrophages with Immunosuppressive Action. *Int J Mol Sci* **25**,
1090 11545 (2024).
1091 42. Hutchison, J. M. *et al.* Recombinant SARS-CoV-2 envelope protein traffics to the trans-Golgi
1092 network following amphipol-mediated delivery into human cells. *J Biol Chem* **297**, 100940 (2021).
1093 43. Hatoyama, Y., Homma, Y., Hiragi, S. & Fukuda, M. Establishment and analysis of conditional
1094 Rab1- and Rab5-knockout cells using the auxin-inducible degron system. *J Cell Sci* **134**, jcs259184
1095 (2021).
1096 44. McLauchlan, H. *et al.* A novel role for Rab5-GDI in ligand sequestration into clathrin-coated pits.
1097 *Curr Biol* **8**, 34–45 (1998).
1098

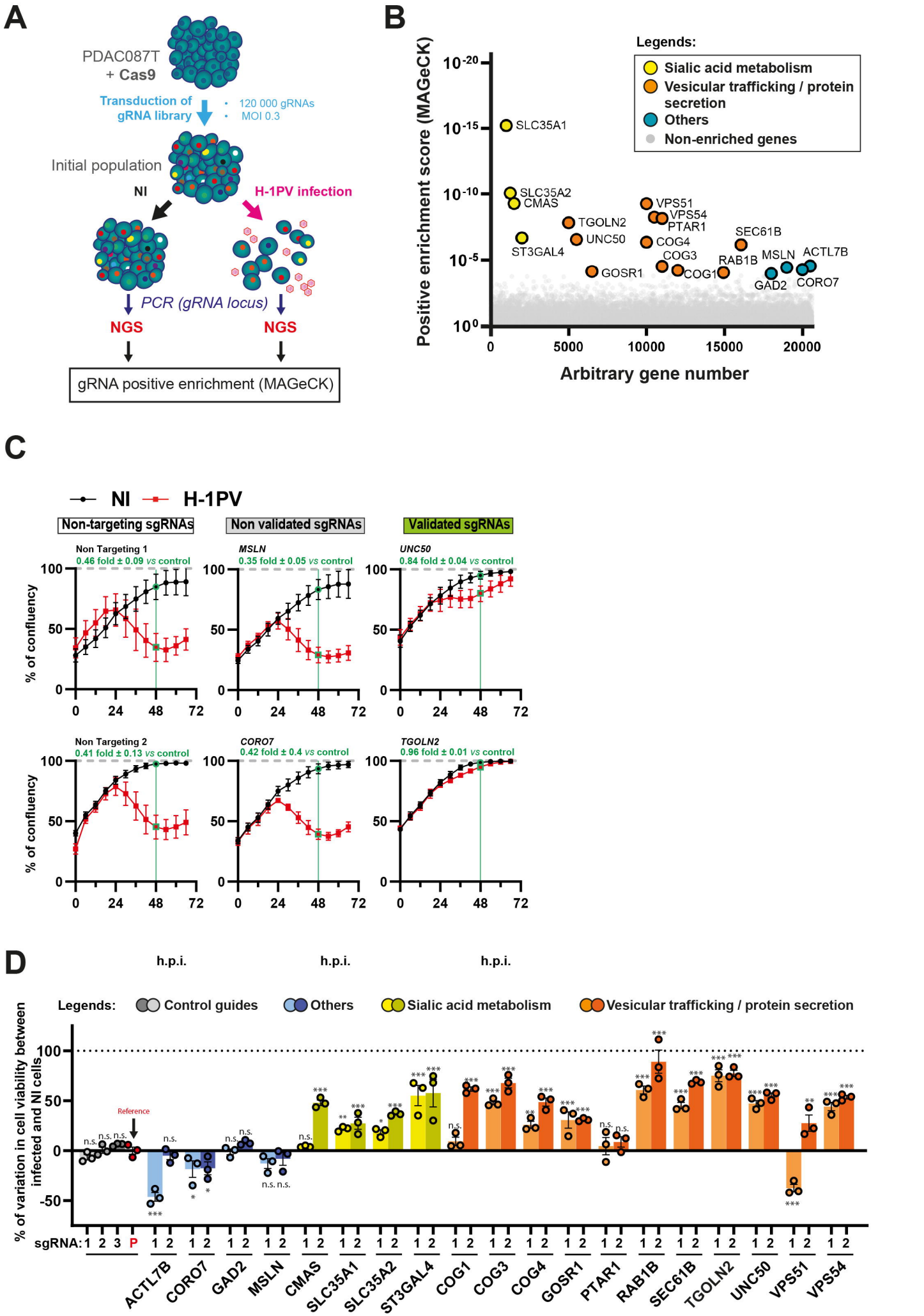
A
PDAC087T
+ Cas9
Transduction of
gRNA library
120 000 gRNAs
MOI 0.3
Initial population
NI
H-1PV infection
PCR (gRNA locus)
NGS
NGS
gRNA positive enrichment (MAGeCK)
B
Legends:
Sialic acid metabolism
Vesicular trafficking / protein secretion
Others
Non-enriched genes
Positive enrichment score (MAGeCK)
Arbitrary gene number
SLC35A1
SLC35A2
CMAS
ST3GAL4
TGOLN2
UNC50
GOSR1
VPS51
VPS54
PTAR1
COG4
COG3
COG1
SEC61B
RAB1B
MSLN
GAD2
ACTL7B
CORO7
C
NI
H-1PV
Non-targeting sgRNAs
Non validated sgRNAs
Validated sgRNAs
Non Targeting 1
0.46 fold ± 0.09 vs control
MSLN
0.35 fold ± 0.05 vs control
UNC50
0.84 fold ± 0.04 vs control
Non Targeting 2
0.41 fold ± 0.13 vs control
CORO7
0.42 fold ± 0.4 vs control
TGOLN2
0.96 fold ± 0.01 vs control
% of confluency
D
h.p.i.
Legends:
Control guides
Others
Sialic acid metabolism
Vesicular trafficking / protein secretion
% of variation in cell viability between infected and NI cells
Reference
sgRNA:
ACTL7B
CORO7
GAD2
MSLN
CMAS
SLC35A1
SLC35A2
ST3GAL4
COG1
COG3
COG4
GOSR1
PTAR1
RAB1B
SEC61B
TGOLN2
UNC50
VPS51
VPS54

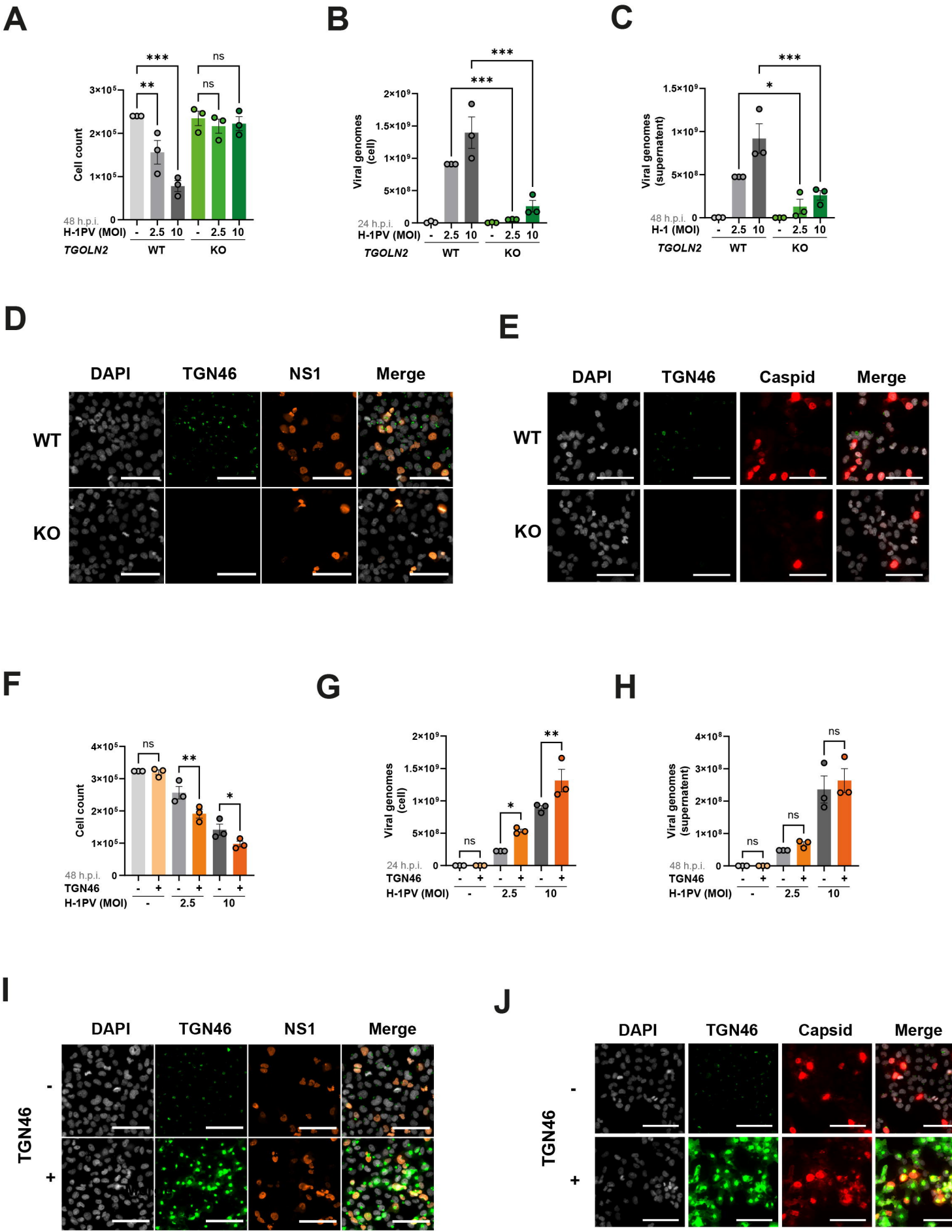
A
Cell count
3×10^5
2×10^5
1×10^5
0
48 h.p.i.
***
**
ns
ns
H-1PV (MOI)
-
2.5
10
-
2.5
10
TGOLN2
WT
KO
B
Viral genomes (cell)
2×10^9
1.5×10^9
1×10^9
5×10^8
0
24 h.p.i.
***
***
H-1PV (MOI)
-
2.5
10
-
2.5
10
TGOLN2
WT
KO
C
Viral genomes (supernatant)
1.5×10^9
1×10^9
5×10^8
0
48 h.p.i.
***
*
H-1 (MOI)
-
2.5
10
-
2.5
10
TGOLN2
WT
KO
D
DAPI
TGN46
NS1
Merge
WT
KO
E
DAPI
TGN46
Caspid
Merge
WT
KO
F
Cell count
4×10^5
3×10^5
2×10^5
1×10^5
0
48 h.p.i.
ns
**
*
TGN46
-
+
-
+
-
+
H-1PV (MOI)
-
2.5
10
G
Viral genomes (cell)
2×10^9
1.5×10^9
1×10^9
5×10^8
0
24 h.p.i.
ns
*
**
TGN46
-
+
-
+
-
+
H-1PV (MOI)
-
2.5
10
H
Viral genomes (supernatant)
4×10^8
3×10^8
2×10^8
1×10^8
0
48 h.p.i.
ns
ns
ns
TGN46
-
+
-
+
-
+
H-1PV (MOI)
-
2.5
10
I
DAPI
TGN46
NS1
Merge
TGN46
-
+
J
DAPI
TGN46
Capsid
Merge
TGN46
-
+

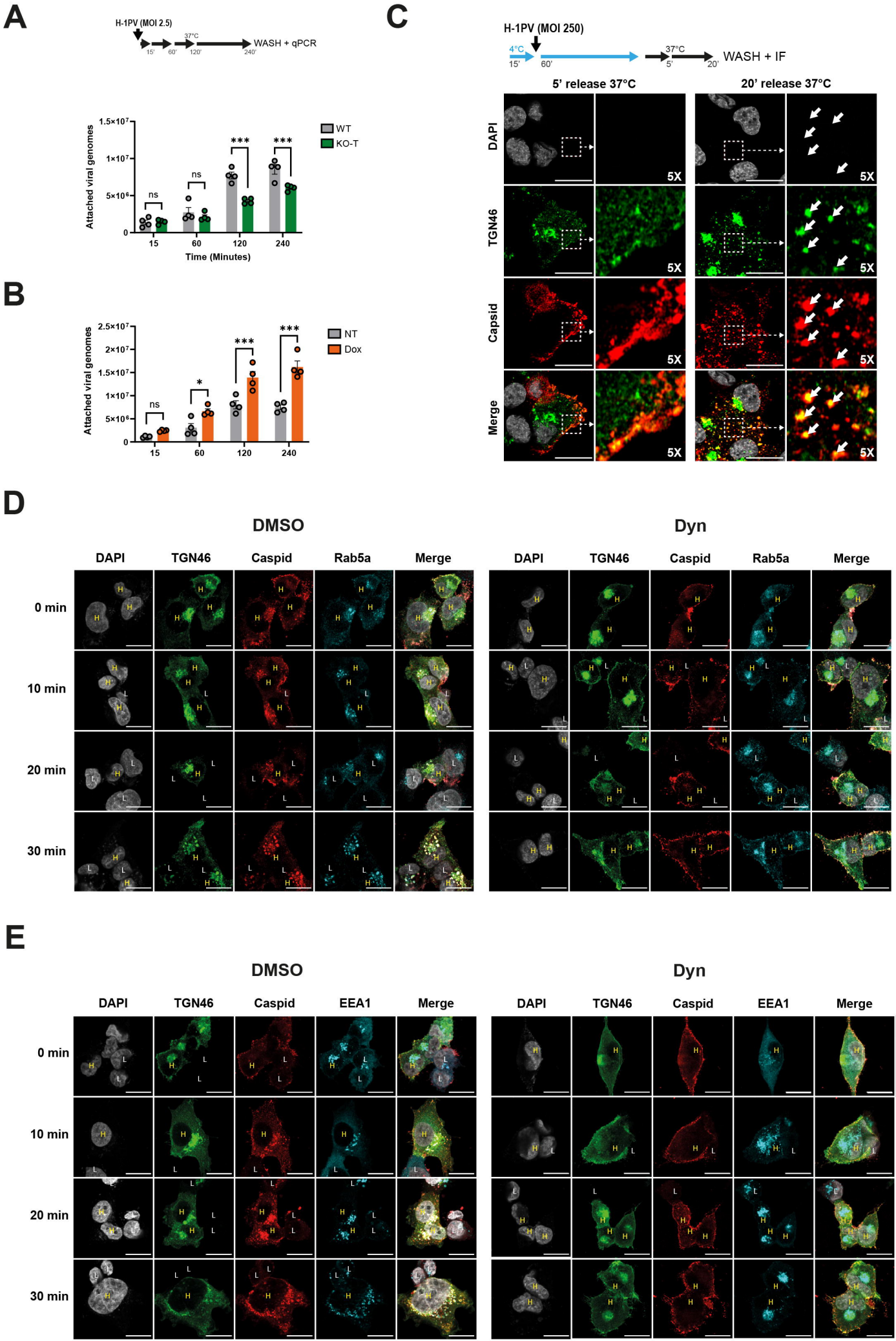
A
H-1PV (MOI 2.5)
15'
60'
37°C
120'
240'
WASH + qPCR
Attached viral genomes
1.5×10⁷
1×10⁷
5×10⁶
0
ns
ns
***
***
WT
KO-T
15
60
120
240
Time (Minutes)
B
Attached viral genomes
2.5×10⁷
2×10⁷
1.5×10⁷
1×10⁷
5×10⁶
0
ns
*
***
***
NT
Dox
15
60
120
240
C
H-1PV (MOI 250)
4°C
15'
60'
37°C
5'
20'
WASH + IF
5' release 37°C
20' release 37°C
DAPI
TGN46
Capsid
Merge
5X
D
DMSO
Dyn
DAPI
TGN46
Caspid
Rab5a
Merge
0 min
10 min
20 min
30 min
H
L
E
DMSO
Dyn
DAPI
TGN46
Caspid
EEA1
Merge
0 min
10 min
20 min
30 min
H
L

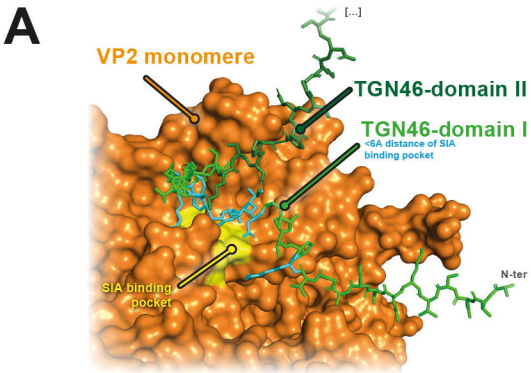
A
VP2 monomere
TGN46-domain II
TGN46-domain I
<6A distance of SIA binding pocket
SIA binding pocket
N-ter

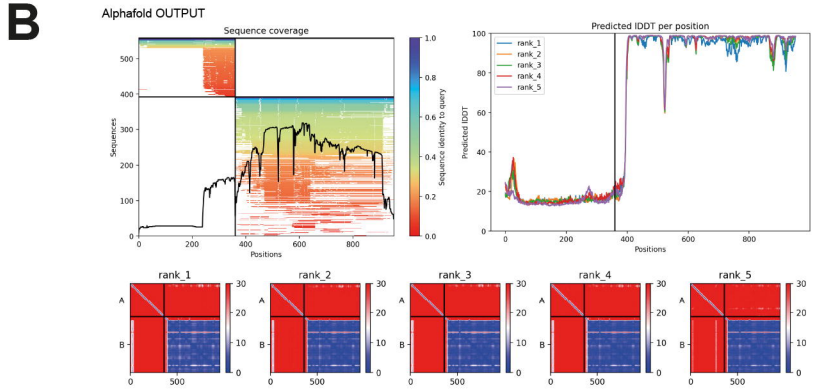
B
Alphafold OUTPUT
Sequence coverage
Sequences
Positions
Sequence identity to query
Predicted lDDT per position
Predicted lDDT
rank_1
rank_2
rank_3
rank_4
rank_5

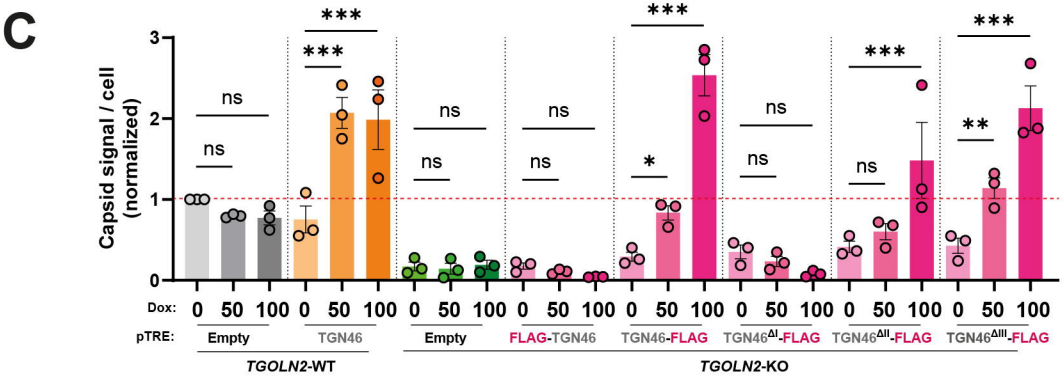
C
Capsid signal / cell (normalized)
Dox:
pTRE:
Empty
TGN46
FLAG-TGN46
TGN46-FLAG
TGN46ΔI-FLAG
TGN46ΔII-FLAG
TGN46ΔIII-FLAG
TGOLN2-WT
TGOLN2-KO
ns
*
**
***

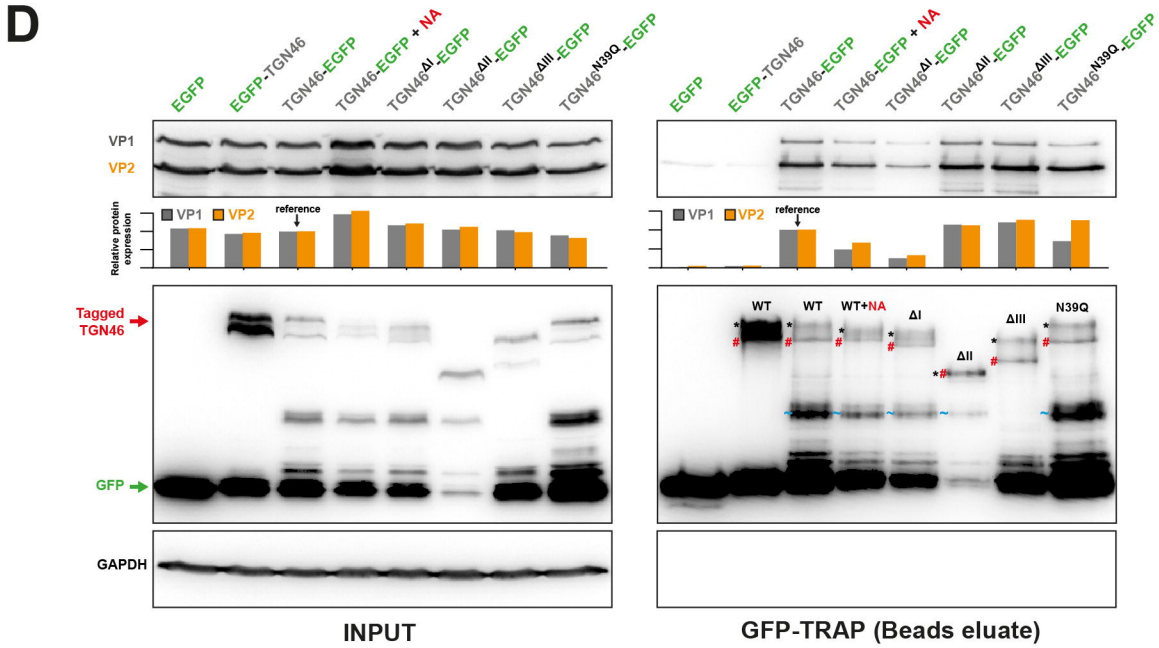
D
EGFP
EGFP-TGN46
TGN46-EGFP
TGN46-EGFP + NA
TGN46ΔI-EGFP
TGN46ΔII-EGFP
TGN46ΔIII-EGFP
TGN46N39Q-EGFP
VP1
VP2
Relative protein expression
reference
Tagged TGN46
GFP
GAPDH
WT
WT+NA
ΔI
ΔII
ΔIII
N39Q
INPUT
GFP-TRAP (Beads eluate)

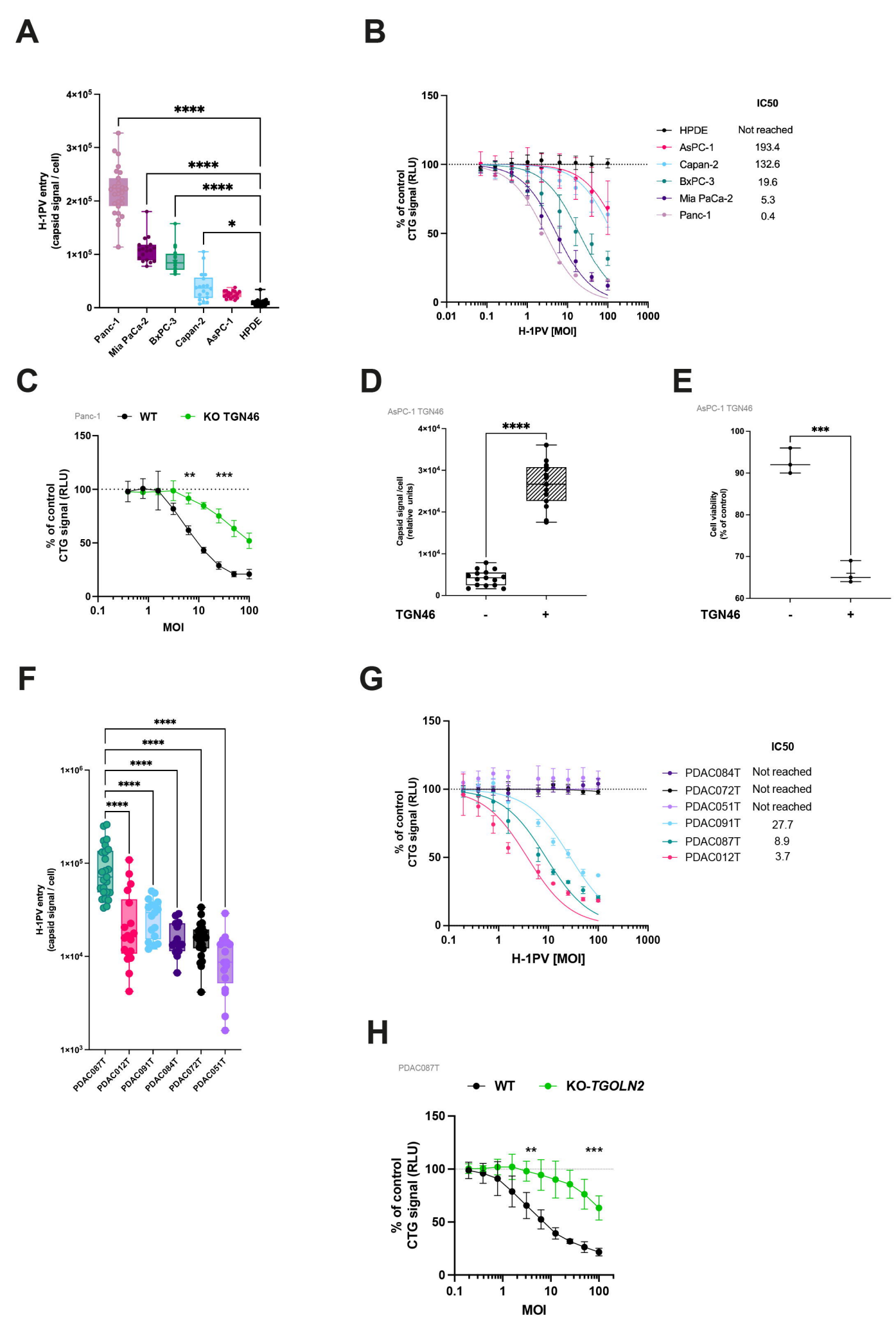
A
H-1PV entry (capsid signal / cell)
4×10^5
3×10^5
2×10^5
1×10^5
0
****
****
****
*
Panc-1
Mia PaCa-2
BxPC-3
Capan-2
AsPC-1
HPDE
B
% of control CTG signal (RLU)
150
100
50
0
0.01
0.1
1
10
100
1000
H-1PV [MOI]
IC50
HPDE Not reached
AsPC-1 193.4
Capan-2 132.6
BxPC-3 19.6
Mia PaCa-2 5.3
Panc-1 0.4
C
Panc-1
WT
KO TGN46
% of control CTG signal (RLU)
150
100
50
0
**
***
0.1
1
10
100
MOI
D
AsPC-1 TGN46
Capsid signal /cell (relative units)
4×10^4
3×10^4
2×10^4
1×10^4
0
****
TGN46
-
+
E
AsPC-1 TGN46
Cell viability (% of control)
100
90
80
70
60
***
TGN46
-
+
F
H-1PV entry (capsid signal / cell)
1×10^6
1×10^5
1×10^4
1×10^3
****
****
****
****
****
PDAC087T
PDAC012T
PDAC091T
PDAC084T
PDAC072T
PDAC051T
G
% of control CTG signal (RLU)
150
100
50
0
0.1
1
10
100
1000
H-1PV [MOI]
IC50
PDAC084T Not reached
PDAC072T Not reached
PDAC051T Not reached
PDAC091T 27.7
PDAC087T 8.9
PDAC012T 3.7
H
PDAC087T
WT
KO-TGOLN2
% of control CTG signal (RLU)
150
100
50
0
**
***
0.1
1
10
100
MOI

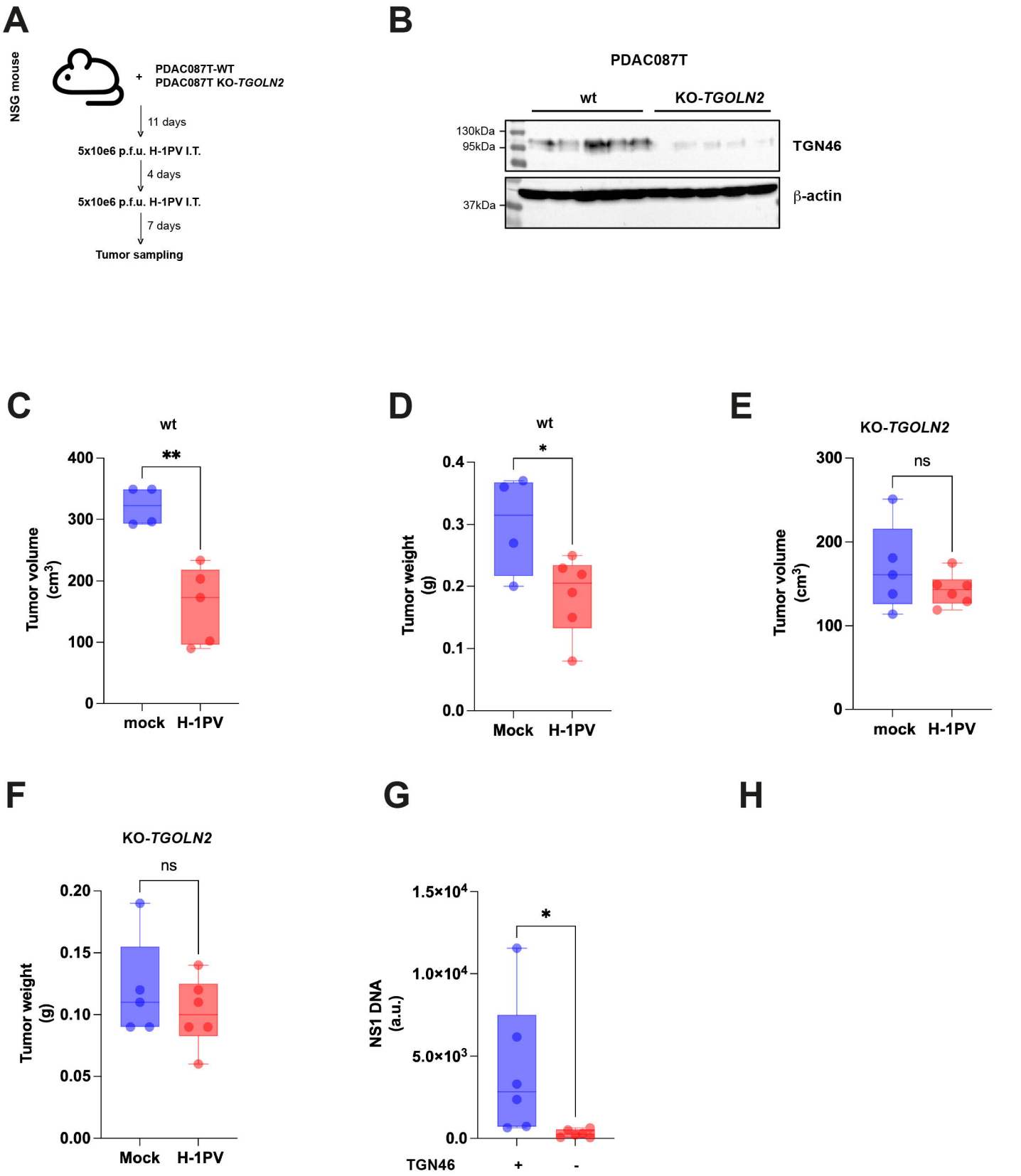
A
NSG mouse
+
PDAC087T-WT
PDAC087T KO-TGOLN2
11 days
5x10e6 p.f.u. H-1PV I.T.
4 days
5x10e6 p.f.u. H-1PV I.T.
7 days
Tumor sampling
B
PDAC087T
wt
KO-TGOLN2
130kDa
95kDa
TGN46
37kDa
β-actin
C
wt
**
Tumor volume (cm3)
400
300
200
100
0
mock
H-1PV
D
wt
*
Tumor weight (g)
0.4
0.3
0.2
0.1
0.0
Mock
H-1PV
E
KO-TGOLN2
ns
Tumor volume (cm3)
300
200
100
0
mock
H-1PV
F
KO-TGOLN2
ns
Tumor weight (g)
0.20
0.15
0.10
0.05
0.00
Mock
H-1PV
G
*
NS1 DNA (a.u.)
1.5×10^4
1.0×10^4
5.0×10^3
0.0
TGN46
+
-
H